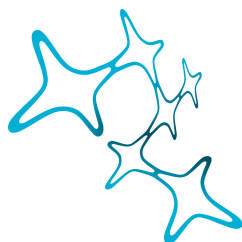


ABHISHEK MISHRA

NEURAL INFORMATION  
PROCESSING IN THE  
*DROSOPHILA* MOTION  
VISION PATHWAY



Graduate School of  
Systemic Neurosciences  
LMU Munich

Dissertation der Graduate School of Systemic Neurosciences der  
Ludwig-Maximilians-Universität München

11<sup>th</sup> of March, 2022

Abhishek Mishra

*Neural information processing in the Drosophila motion vision pathway*

Dissertation der Graduate School of Systemic Neurosciences der  
Ludwig-Maximilians-Universität München.

E-MAIL:

[amishra@neuro.mpg.de](mailto:amishra@neuro.mpg.de)

11<sup>th</sup> of March, 2022

---

*First reviewer and supervisor*  
Prof. Dr. Alexander Borst

*Second reviewer*  
Prof. Dr. Ruben Portugues

*Date of submission*  
11<sup>th</sup> of March, 2022



# CONTENTS

<b>1</b>	<b>INTRODUCTION</b>	<b>1</b>
1.1	<i>Drosophila</i> as a model organism	1
1.2	Tools for functional dissection of <i>Drosophila</i> neural circuits	1
1.2.1	GAL4-UAS / LexA-lexAop	1
1.2.2	Calcium Indicator : GCaMP for recording changes in intracellular calcium	2
1.2.3	Voltage Indicator : Arclight for recording changes in neuronal membrane potential	2
1.2.4	Suppressor : shibire <sup>ts</sup> , GtACR for silencing neuron	4
1.2.5	Activator : ReaChr for activating neuron	5
1.3	Neural communication	5
1.3.1	Electrical synapses	5
1.3.2	Chemical synapses	6
1.3.3	Voltage-gated ion channels	6
1.4	Fly motion vision system	8
1.4.1	Parallel ON and OFF processing pathways	10
1.4.2	T4 and T5 cells	11
1.5	Neural circuit underlying direction selectivity	11
1.6	Neural algorithm underlying direction selectivity	13
<b>2</b>	<b>PUBLICATIONS</b>	<b>15</b>
2.1	A common directional tuning mechanism of <i>Drosophila</i> motion-sensing neurons in the ON and in the OFF pathway	15
2.2	Voltage to Calcium Transformation Enhances Direction Selectivity in <i>Drosophila</i> T4 neurons	33
Bibliography		51

# LIST OF FIGURES

Figure 1	Genetic tools for functional manipulations in <i>Drosophila</i>	3
Figure 2	Chemical synapse: steps of synaptic transmission	7
Figure 3	Voltage-gated ion channels	8
Figure 4	Fly optic lobe	9
Figure 5	t4t5inputsynapses	12



# 1

## INTRODUCTION

### 1.1 *Drosophila* AS A MODEL ORGANISM

*Drosophila melanogaster* is one of the most powerful model organisms available for functional dissection of neural circuits. It allows for most sophisticated in vivo neural manipulations - imaging, activation and suppression of neural activity. Over 100 years of research in *Drosophila* has allowed generation of thousands of fly 'driver-lines' which can be used to express genes of interest in neuron-specific manner (Pfeiffer *et al.* 2008). Along with this, *Drosophila* allows several practical working advantages: They are small, has a short generation time of about 10 days and easy to grow in a lab.

*Drosophila* brain is estimated to contain about 100,000 neurons (Zheng *et al.* 2018). *Drosophila* brain involves computation of modest complexity. These computations are implemented in circuits that contain a limited number of neurons, and with *Drosophila* genetic armoury almost each of these neuron can be precisely targeted. However even with comparatively less complexity, there are surprising parallels between how fly and mammalian brains process information (Borst & Helmstaedter 2015). Insights about the nervous system obtained in *Drosophila* is thus often relevant for other species (Bellen *et al.* 2010; Venken *et al.* 2011).

### 1.2 TOOLS FOR FUNCTIONAL DISSECTION OF *Drosophila* NEURAL CIRCUITS

To have a detailed understanding of how a neural circuit functions, we need to know role each individual neuron plays in that particular circuit. To achieve this, we would like to perform following three types of manipulations on the given neuron: (i) record neuronal activity from the neuron, (ii) activate the neuron and (iii) silence the neuron. Fortunately years of research in *Drosophila* has provided us with multiple tools in order to be able to perform these manipulations in the choice of neuron we want. The most important tool which enables us to do this in neuron-specific manner is the Gal4-UAS system (figure 1).

#### 1.2.1 GAL4-UAS / LexA-lexAop

Following the discovery of transposable DNA sequences (P-elements) in the *Drosophila* genome (Rubin & Spradling 1982), Brand & Perrimon 1993 designed GAL4-UAS system. The GAL4-UAS system is the workhorse of *Drosophila* genetics. The GAL4-UAS system is a binary expression system consisting of two main components: the yeast transcriptional factor GAL4

expressed in a specific pattern and a reporter gene under the control of UAS promoter that is silent in the absence of GAL4. Gal4-UAS system essentially involves crossing two fly lines: one called the 'driver-line', defines which neurons express required effector gene; the other called 'reporter-line', defines what gene is expressed in the neurons defined by driver line.

Another independent binary transcriptional system which can be used is LexA-lexAop system. This method is based on the bacterial DNA-binding operator lexAop and controlled by the expression of LexA. LexA binds to and activates the lexA operator (lexAop). We can use LexA-lexAop system in combination with GAL4-UAS system to simultaneously express gene of interest in two different neuronal population. Using combination of GAL4-UAS and LexA-lexAop system, we can express following three types of reporter genes: Indicator, Suppressor & Activator.

### **1.2.2 Calcium Indicator : GCaMP for recording changes in intracellular calcium**

To record neuronal activity, one can use GAL4-UAS system to express GFP in the required neuron, and then use somatic patch recording to record neural activity from the neuron (Wilson *et al.* 2004; Joesch *et al.* 2008). However, neurons in the optic lobe of *Drosophila* are often too small in size for successful electrophysiological recording. To overcome this we can use calcium indicators as proxy for neuronal activity (figure 1a).

Neural activity causes rapid changes in intracellular free calcium (Baker *et al.* 1971; Egelhaaf & Borst 1995; Sabatini *et al.* 2002). We can thus express genetically encoded calcium indicators (GECIs) which changes its fluorescence according to the change in concentration of intracellular calcium. GECIs typically consist of a calcium-binding domain - calmodulin, calmodulin-binding peptide M13, and a reporter element which is based on either a single fluorescent protein or two fluorescent proteins (Broussard *et al.* 2014). In the case of single fluorescent protein for example in GCaMPs, calmodulin (CaM) binds the M13 peptide in the presence of calcium. This coupling results in conformational changes in the fluorescent protein, resulting in change in fluorescence intensity (Nagai *et al.* 2001). In the case of two fluorescent proteins, conformational changes lead to Fluorescence Resonance Energy Transfer (FRET) between two fluorescent proteins with overlapping excitation and emission spectra (Miyawaki *et al.* 1997). In this thesis, we use GCaMP6f (T.-W. Chen *et al.* 2013) in combination with two-photon microscopy for recording neural activity.

### **1.2.3 Voltage Indicator : Arclight for recording changes in neuronal membrane potential**

In order to measure the membrane potential changes in neurons, electrophysiology has been the most frequently used method. However, due to the small size of neurons in the optic lobe, single-cell electrophysiological recordings of these neurons have been difficult. Genetically encoded voltage indicators (GEVIs) have evolved as powerful tools for recording changes in

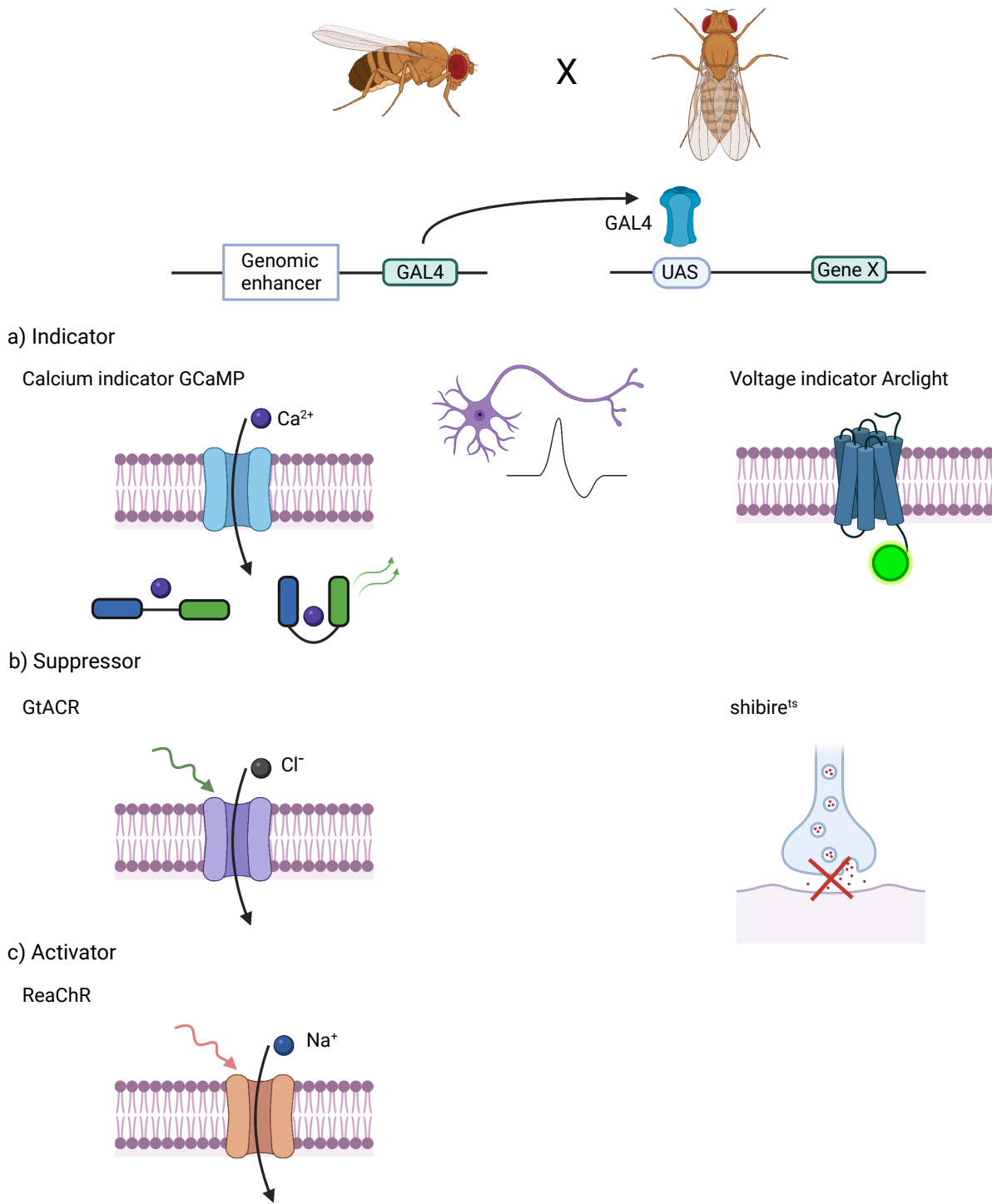


**Figure 1:** The Gal4-UAS system is used to express a gene of interest in a specific subset of neurons. (a) Calcium indicator is used to record neural activity using intracellular calcium concentration. Voltage indicator is used to optically record membrane potential changes in the neuron. (b) Neural activity can be suppressed by expressing light sensitive chloride channels or by blocking synaptic transmission via expression of temperature-sensitive *shibire<sup>ts</sup>*. (c) Neurons can be activated via expression of light-sensitive cation channels. (modified from Borst 2009)

neuronal membrane potentials. Optical methods of monitoring brain activity are appealing because they allow simultaneous, noninvasive monitoring of activity in many individual neurons and different parts of the brain.

We use a fluorescence protein (FP) voltage sensor called Arclight (Jin *et al.* 2012). Arclight is based on the fusion of voltage sensing domain of *Ciona intestinalis* voltage sensitive phosphatase (Murata *et al.* 2005) and the fluorescent protein super ecliptic pHluorin with an A227D mutation. Arclight's fluorescence decreases with membrane depolarization and increases with membrane hyperpolarization. We used Arclight in combination with two-photon imaging to record changes in neuronal membrane potential.

#### 1.2.4 Suppressor : shibire<sup>ts</sup>, GtACR for silencing neuron

In order to understand the principles of information processing in a neural circuit, along with recording neural activity we would also like to either suppress or activate neural activity in other neurons in the circuit. Inactivation and activation of genetically defined cell types help establish causal relations in specific group of neurons and neural circuit. There are several tools which allow for inactivation of a neuron. Cell death genes such as *reaper* (*rpr*) and *head involution defective* (*hid*) or *grim* induce apoptosis (Grether *et al.* 1995; P. Chen *et al.* 1996). The tetanus toxin light chain (TeTxLc) cleaves the synaptic vesicle protein synaptobrevin, and inhibits neurotransmitter exocytosis at chemical synapses (Sweeney *et al.* 1995). The expression of Kir - an inwardly rectified potassium channel causes neurons to hyperpolarize, resulting in suppressed excitability (Johns *et al.* 1999). While using Gal4-UAS system to express these effectors provide effective control over the functionality of the targeted neurons, it also creates some unwanted problems. First, because most enhancers are active at several stages of development, it is difficult to avoid the toxic effects of expressed gene product on development. Second, if particular neurons are eliminated during development, their loss in function may be compensated by some other neuron, hence making interpretation of results difficult. third, it is not possible to observe acute effect elicited by the temporal inactivation of particular neurons. To overcome these limitations, we can use conditional effector proteins like shibire<sup>ts</sup> & GtACR (figure 1b), which is activated by higher temperature & light respectively.

*Drosophila shibire* encodes the protein dynamin, which is involved in the process of endocytosis and is essential for vesicle recycling. The dominant-negative temperature sensitive allele shibire<sup>ts</sup> is defective in synaptic vesicle recycling at restrictive temperature ( $> 29^{\circ}\text{C}$ ) which results in rapid and reversible inhibition of synaptic transmission (Kitamoto 2001). In *Drosophila*, Joesch *et al.* 2010 showed that flies expressing shibire<sup>ts</sup> if exposed to persistent heat-shock for one hour at restrictive temperature ( $37^{\circ}\text{C}$ ), the output of affected cells is suppressed for several hours. This experimental method gives us a longer time duration, which allows us to record neural activity from the fly while the activity from the neuron expressing shibire<sup>ts</sup> is suppressed. However, we get this extra time duration at the cost of losing reversibility of activity.

The tools we have mentioned above allows for a cell-type-specific neuro-modulation. However, in addition to the cell-type-specificity we would also like to have temporally accurate and reversible neuromodulation. *Guillardia theta* Anion Channel Rhodopsins (GtACR1 and GtACR2) can provide us with these additional advantages (Govorunova *et al.* 2015). GtACRs impart strong light-gated chloride conductance and is much more light-sensitive than Halorhodopsin class of chloride pumps. In particular with respect to the fly visual system, we used GtACR1 since its activation spectrum is shifted towards longer wavelengths with respect to five of the six *Drosophila* rhodopsins (except rhodopsin 6) (Mauss *et al.* 2017; Mohammad *et al.* 2017). Thus, we can use Gal4-UAS system to express GtACR in neurons we want to hyperpolarize & silence the neural activity. Simultaneously, we can express GCaMP in downstream neurons using LexA-lexAop system & record their neural activity, while silencing the neurons expressing GtACR.

### 1.2.5 Activator : ReaChr for activating neuron

Along with using GCaMP for imaging, shibire<sup>ts</sup> or GtACR for suppressing neural activity, we would also like to have a tool for activating neuron. Ideal method for activation requires excellent temporal control. Light-gated cation channels - Channelrhodopsins(ChRs) can be used for this purpose (figure 1c). ChRs are light-gated, non-specific cation channels that allow selective depolarization of genetically targeted cells. Here we have used red-activatable ChR (ReaChr), a variant of ChR (Lin *et al.* 2013; Busch *et al.* 2018).

Therefore by combining the use of GCaMP for calcium imaging and GtACR for suppression or ReaChR for activation, we can better understand the functions of neurons present in a given neural circuit.

## 1.3 NEURAL COMMUNICATION

Camillo Golgi's silver-stain method made it possible to visualize the nervous system in tissue samples under the light microscope around 1873. Santiago Ramón y Cajal in 1888 described the nervous system as a network of individual cells. About a decade later, in 1897, the term 'synapse', derived from the Greek word 'synapsis' (meaning 'conjunction'), was used to describe the connections between two neurons. Neurons form networks where they communicate via synapses. Two types of synapses exist: 1) Electrical synapses 2) Chemical synapses

### 1.3.1 Electrical synapses

In electrical synapses, two cells are directly connected by cluster of intercellular channels called gap junctions (Bennett & Zukin 2004). The gap junctions provide a conductive pathway for electrical current to spread between cells that are interconnected. Consequently, electrical currents underlying action potentials or graded potentials directly propagate to postsynaptic neurons, with a similar time course to presynaptic signals. Additionally, since elec-

trical signals propagate bidirectionally, signalling events generated in the postsynaptic cells also spread to the presynaptic cells. In *Drosophila*, electrical synapses are widely distributed throughout the nervous system and are essential to neuronal function (Ammer *et al.* 2022).

### 1.3.2 Chemical synapses

Neurons communicate mostly via chemical synapses (figure 2) which requires the release of neurotransmitters. When the presynaptic membrane is sufficiently depolarized, voltage-gated calcium channels open and allow  $\text{Ca}^{2+}$  to enter the cell (Luo 2020). Calcium entry leads to the fusion of synaptic vesicles with the membrane and release of neurotransmitter molecules into the synaptic cleft (Chapman 2002). As neurotransmitters diffuse across the synaptic cleft, they bind to receptors in the postsynaptic membrane, causing postsynaptic neuron to depolarize or hyperpolarize, passing the information from pre to postsynaptic neurons (Di Maio 2008). Voltage to calcium transformation in neurons is therefore a crucial step in neural information processing and neural computation.

### 1.3.3 Voltage-gated ion channels

Voltage-gated ion channels are transmembrane proteins that allow certain inorganic ions to cross cell membranes (figure 3). Generally, these channels consist of two distinct but functionally coupled transmembrane domains: the voltage sensing domain and the pore domain. The voltage sensing domain changes the confirmation of the pore domain in response to changes in transmembrane potential, allowing selected ions to flow down their electrochemical gradient.

**VOLTAGE-GATED CALCIUM CHANNELS** Voltage-gated calcium channels mediate depolarization-induced calcium influx that drives release of neurotransmitter. The  $\alpha 1$ -subunit of the voltage-gated calcium channels forms the ion-conducting pore, which makes it distinct from other calcium channels. Three families of genes encode  $\alpha 1$  subunits. *Drosophila* genome has one  $\alpha 1$  subunit gene in each family:  $\alpha 1D$  ( $\text{Ca}_v1$ ),  $cac$  ( $\text{Ca}_v2$ ), and  $\alpha 1T$  ( $\text{Ca}_v3$ ) (Litton & Ganetzky 2000; King 2007). In *Drosophila* antennal lobe projection neurons,  $cac$  ( $\text{Ca}_v2$ ) type and  $\alpha 1T$  ( $\text{Ca}_v3$ ) type voltage-gated calcium channels are involved in sustained and transient calcium currents, respectively (Gu *et al.* 2009; Iniguez *et al.* 2013).

**VOLTAGE-GATED SODIUM CHANNELS** In neurons, voltage-gated sodium channels play a crucial role in the initiation and propagation of action potentials (Hodgkin & Huxley 1952). Sodium channels are activated and deactivated within milliseconds when the membrane is depolarized by a few millivolts. There are at least ten genes in mammals that encode these large membrane proteins. In contrast, *paralytic* (*para*) is the only voltage-gated sodium channel gene described in *Drosophila*. Loss of *paralytic* (*para*) reduces neuroblast progeny cell number in *Drosophila* (Piggott *et al.* 2019).

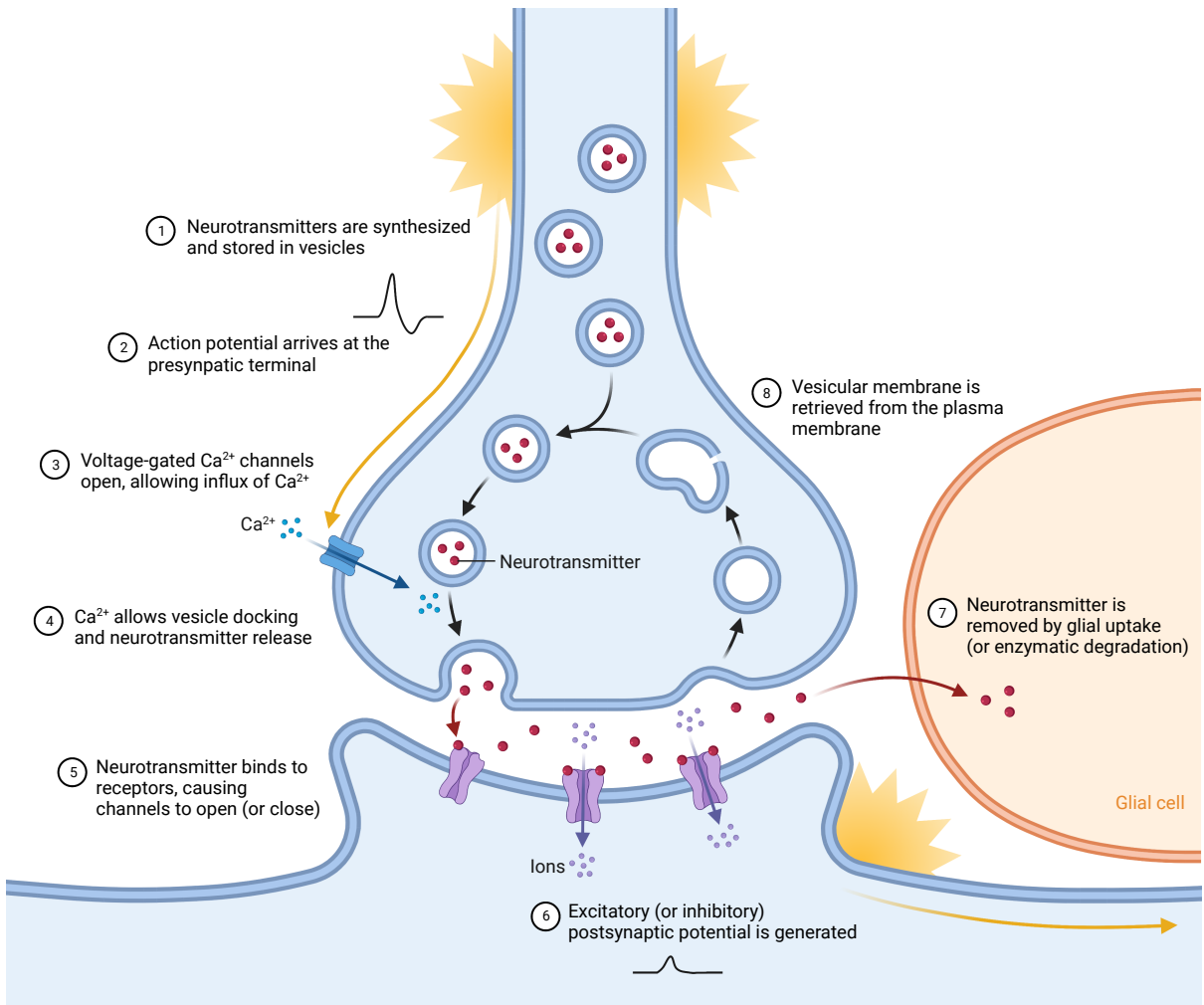


**Figure 2:** Chemical synapse: steps of synaptic transmission. (1) Synthesis and storage of neurotransmitter in the vesicles. (2) Depolarization in the presynaptic terminal causes (3) voltage-gated calcium channels to open and allow influx of calcium ions. (4) High concentration of calcium ions trigger the fusion of neurotransmitter filled vesicles with the presynaptic membrane and release of neurotransmitters into the synaptic cleft. (5) Neurotransmitters released in the synaptic cleft bind to receptors in the postsynaptic membrane leading to (6) excitatory or inhibitory postsynaptic potential. (figure created with [Biorender.com](#))

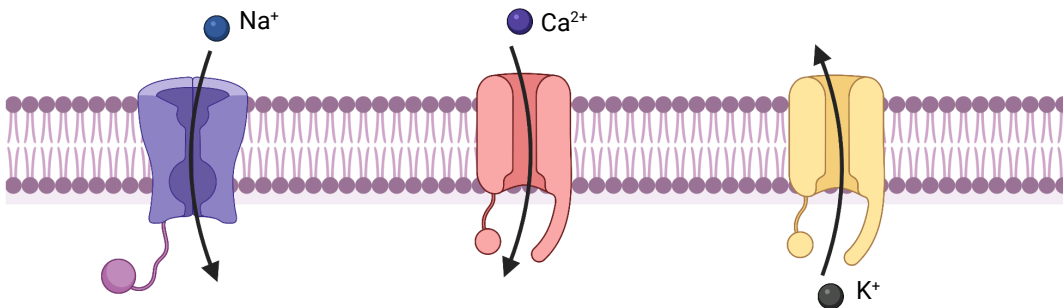


**Figure 3:** Voltage-gated ion channels: The sodium channels allow  $\text{Na}^+$  ions to enter into the cell. The calcium channels allow  $\text{Ca}^{2+}$  ions to enter into the cell. The potassium channels allow efflux of the  $\text{K}^+$  ions.

**VOLTAGE-GATED POTASSIUM CHANNELS** Voltage-gated potassium channels are transmembrane channels specific for potassium ions. They play a crucial role in returning the depolarized cell to its resting membrane potential, after each action potential. Voltage-gated potassium channels are the most diverse family of voltage-gated ion channels in the human genome, with 40 members for  $\alpha$  subunit grouped into 12 families (Gutman *et al.* 2005). The first voltage-gated potassium channel discovered in the *Drosophila* was *Shaker* (Papazian *et al.* 1987). Afterwards, three additional *Shaker* like voltage-gated potassium genes were identified in *Drosophila*: *Shab*, *Shaw* and *Shal* (Covarrubias *et al.* 1991).

#### 1.4 FLY MOTION VISION SYSTEM

*Drosophila* visual processing pathway is comprised of retina, lamina, medulla, lobula and lobula plate, each arranged in columnar, retinotopic fashion (figure 4a) (Fischbach & Dittrich 1989). If one were to record from a single photoreceptor in the retina, it would show similar response to a patch of moving image irrespective of the direction of motion: meaning it is not direction-selective. However, if one records around 4 synapses downstream, Lobula Plate Tangential Cells (LPTCs) depolarise in response to a patch of image moving in its preferred direction and hyperpolarize if the image moves in opposite direction or the null direction (figure 4b). HS (Horizontal System) cells for example are responsive to horizontal motion (Schnell *et al.* 2010), while VS (Vertical System) cells are responsive to vertical motion (Joesch *et al.* 2008). LPTCs, however integrate over large parts of visual fields, i.e. they are not local motion detectors. Hence, the natural question arises: which cells are the local motion detectors?

The answer to the above question is: T<sub>4</sub> and T<sub>5</sub> are first local motion detectors found in the *Drosophila* ON and OFF motion vision pathway respectively. Four sub-population of T<sub>4a-d</sub> and T<sub>5a-d</sub> cells tuned to the four cardinal directions and projecting to the four layers in the lobula plate can be found within each column (Maisak *et al.* 2013). This leads to next question: what makes T<sub>4</sub> and T<sub>5</sub> direction selective? To answer this question, we need to investigate the cells which are present in between the non-direction-selective

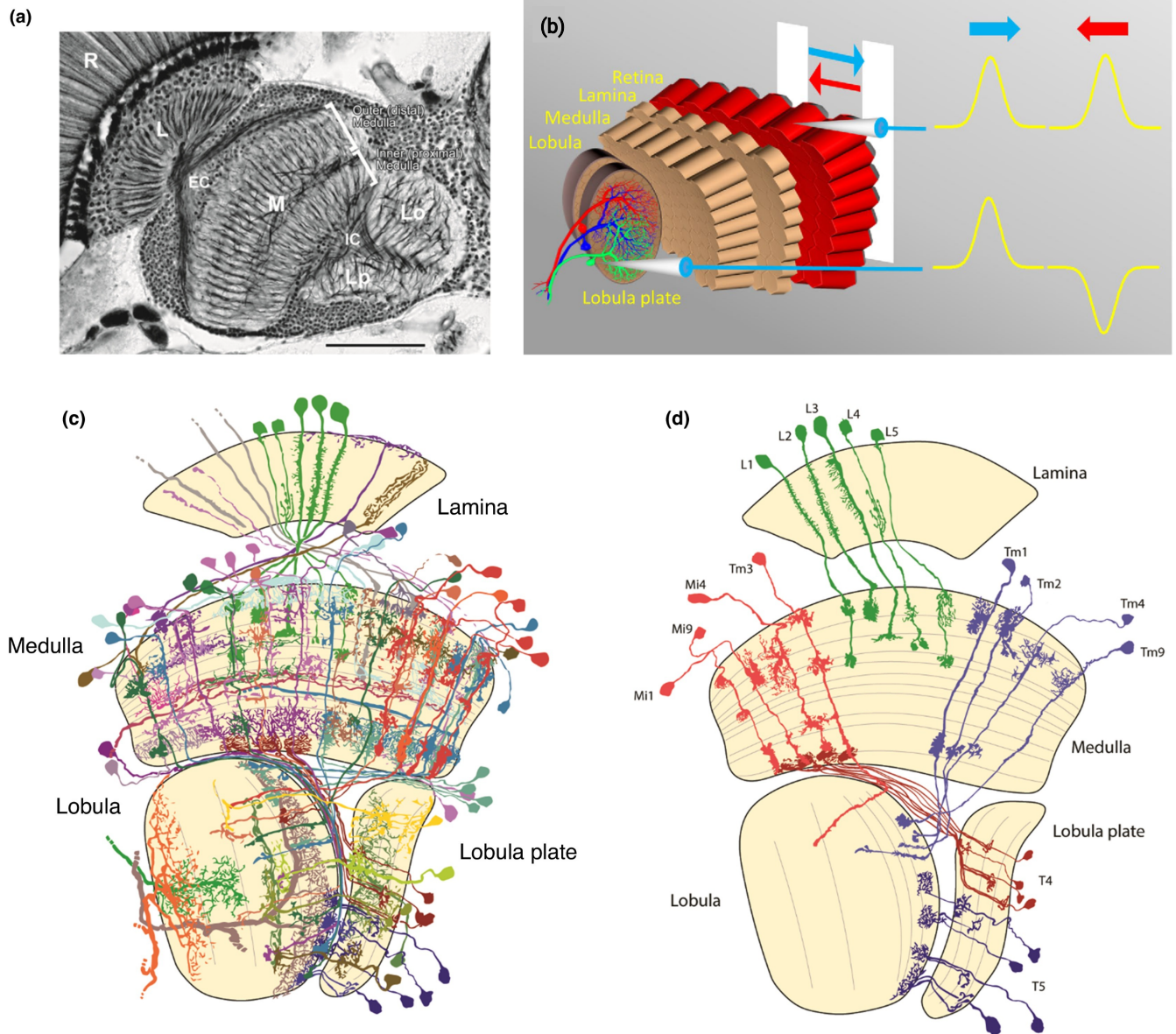


Figure 4: Fly optic lobe

photoreceptors in the retina and direction-selective T<sub>4</sub>, T<sub>5</sub> cells in Medulla and Lobula respectively (figure 4c, d). The columnar cell types of the lamina, medulla, lobula and lobula plate have all been identified and described (Ramón y Cajal & Sánchez 1915; Fischbach & Dittrich 1989).

**LAMINA** Lamina is organized in an array of ~ 750 retinotopic columns (also called 'cartridges'). Each column corresponds to ~ 5° discrete sample of the visual world. Light sensitive photoreceptors, R<sub>1-6</sub> project their axons into each lamina column. Two other photoreceptors, R<sub>7</sub> & R<sub>8</sub> pass through lamina and synapse in specific layers of medulla. Along with photoreceptor axons, lamina includes 5 lamina output neurons (L<sub>1-L5</sub>), six putative feedback neurons (T<sub>1</sub>, Lat, Law<sub>1</sub>, Law<sub>2</sub>, C<sub>2</sub>, C<sub>3</sub>) and one lamina intrinsic neuron (Lai). Lamina columnar monopolar neurons, L<sub>1-L5</sub> send their axonal projections into specific layers of the medulla. (Fischbach & Dittrich 1989; Tuthill et al. 2013).

**MEDULLA** Medulla consists of more than 60 different cell types in a single column. They can be clustered into different groups based on their anatomy. Medulla intrinsic ('Mi') neurons connect different layers of the medulla to each other. Trans-medulla ('Tm') neurons connect specific layers of medulla to various layers in the lobula. Trans-medulla Y ('TmY') neurons connect specific layers of the medulla to various layers in the lobula and lobula plate. The medulla consists of 10 layers, M<sub>1</sub> to M<sub>10</sub>. Directions-selective cell T<sub>4</sub> connects medulla layer 10 to the four layers of lobula plate.

While the circuit was known, the small size of these neurons made electrophysiological recordings difficult. Only after the advent of modern 2-photon imaging in combination with using Gal4-UAS system to express GCaMP in these cells, it became possible to record neuronal activity from these cells. Experiments over the years using these techniques revealed following interesting results : (a) Visual processing in *Drosophila* occur in two parallel processing pathways for brightness increment (ON) and brightness decrement (OFF) (Joesch et al. 2010; Eichner et al. 2011; Joesch et al. 2013; Behnia et al. 2014; Strother et al. 2014) (b) T<sub>4</sub> and T<sub>5</sub> are first local motion detectors found in the *Drosophila* ON & OFF motion vision pathway respectively. Four sub-population of T<sub>4a-d</sub> and T<sub>5a-d</sub> cells tuned to the four cardinal directions and projecting to the four layers in the lobula plate can be found within each column (Maisak et al. 2013).

#### 1.4.1 Parallel ON and OFF processing pathways

In striking similarity to mammalian retina (Masland 2012), visual processing in *Drosophila* occurs in two parallel ON and OFF processing pathways (Borst & Helmstaedter 2015). The ON pathway transmits information about brightness increments, while the OFF pathway transmits information about brightness decrements. In order to understand split of photoreceptor (R<sub>1-R6</sub>) signals into ON and OFF pathway, studies have been done blocking Laminar monopolar cells, while simultaneously recording from downstream LPTCs neuron. While blocking L<sub>1</sub> neurons resulted in specific reduction of LPTC's

response to ON stimulus (brightness increment), blocking L<sub>2</sub> neurons resulted in specific reduction of LPTC's response to OFF stimulus (brightness decrement) (Joesch *et al.* 2010). In behavioral experiments, walking flies were unable to follow either ON or OFF motion when either L<sub>1</sub> or L<sub>2</sub> was blocked respectively (Clark *et al.* 2011; Maisak *et al.* 2013). The flies become completely motion-blind if both L<sub>1</sub> and L<sub>2</sub> are permanently hyperpolarized (via Kir2.1) (Bahl *et al.* 2013; Tuthill *et al.* 2013). These experiments together suggests that L<sub>1</sub> pathway specifically transmits information about brightness increments to downstream ON motion detector, and L<sub>2</sub> pathway specifically transmits information about brightness decrements to downstream OFF motion detector.

#### 1.4.2 T<sub>4</sub> and T<sub>5</sub> cells

Based on previous studies from (Buchner *et al.* 1984; Fischbach & Dittrich 1989), T<sub>4</sub> and T<sub>5</sub> were long thought to be the prime candidates for local motion detectors in the ON and OFF pathway respectively. However, due to its small size it was difficult to do electrophysiological recordings from T<sub>4</sub> and T<sub>5</sub> cells. This problem was solved using combination of 2-photon imaging and Gal4-UAS system to express GCaMP in T<sub>4</sub>, T<sub>5</sub> cells to record its neural activity in response to the ON and OFF stimuli. Stimulating the flies in four cardinal directions (front-back, back-front, upwards and downwards), Maisak *et al.* 2013 recorded direction selective activity from T<sub>4</sub>/T<sub>5</sub> cells. Four sub-population of T<sub>4a-d</sub> and T<sub>5a-d</sub> cells tuned to the four cardinal directions and projecting to the four layers in the lobula plate were found within each column. Further, T<sub>4</sub> were found to respond specifically to ON stimulus and T<sub>5</sub> were found to respond specifically to OFF stimulus. Blocking T<sub>4</sub> and T<sub>5</sub> cells led to a complete loss of motion response in lobula plate tangential cells (Schnell *et al.* 2012), of the optomotor response of tethered walking flies (Bahl *et al.* 2013). Specific blocking of T<sub>4</sub> cells led to reduction in LPTC and optomotor responses to ON stimulus selectively. While specific blocking of T<sub>5</sub> cells led to reduction in LPTC and optomotor responses to OFF stimulus selectively. These results together suggest T<sub>4</sub> and T<sub>5</sub> to be the elementary motion detector for ON and OFF pathway respectively (Maisak *et al.* 2013).

### 1.5 NEURAL CIRCUIT UNDERLYING DIRECTION SELECTIVITY

Having identified T<sub>4</sub> and T<sub>5</sub> as the elementary local motion detectors, the next question which arises is which cells provide synaptic inputs to T<sub>4</sub> and T<sub>5</sub> cells. Electron Microscopy (EM) studies (Shinomiya2019; Takemura2017) provided answer to this question. Shinomiya2019 used FIB-SEM (Focused Ion Beam Serial Electron Microscope) to record a volume of the optic lobe comprising of seven columns of the medulla, lobula and lobula plate. They identified all the different neuron types providing inputs to the T<sub>4</sub> and T<sub>5</sub> cells. T<sub>4</sub> cells receive input from Mi<sub>1</sub>, Tm<sub>3</sub>, Mi<sub>4</sub>, Mi<sub>9</sub>, C<sub>3</sub>, CT<sub>1</sub> and TmY<sub>15</sub>. T<sub>5</sub> cells receive input from Tm<sub>1</sub>, Tm<sub>2</sub>, Tm<sub>4</sub>, Tm<sub>9</sub>, CT<sub>1</sub>, TmY<sub>15</sub>, LT<sub>33</sub> and

Tm23. T4 and T5 cells' dendrites span over several columns along the preferred direction of the motion. The authors could also locate where the different cell type synapse onto the dendrites of T4 and T5. For example for T4c with preferred direction of motion as upwards receives input from Mi1, Tm3 and TmY15 in the central part of its dendrite, from Mi9 and T4c on the ventral part and from Mi4, C3 and CT1 on the dorsal part of its dendrite [figure 5 top]. For T4d with preferred direction as downwards, it receives input from Mi1, Tm3 and TmY15 in the central part, from Mi9 and T4d on the dorsal part and from Mi4, C3, CT1 on the ventral part of its dendrite. In summary, all T4 subtypes receive inputs from Mi1, Tm3 and TmY15 in the central part, from Mi9 on the preferred side (i.e. the side from which a preferred direction stimulus approaches) and from Mi4, C3 and CT1 on the null side (i.e. the side from which a null direction stimulus approaches) of their dendrite. Similarly, all T5 subtypes receive inputs from Tm1, Tm2 and Tm4 on the central part, Tm9 on the preferred side and CT1 on the null side of their dendrite [figure 5].

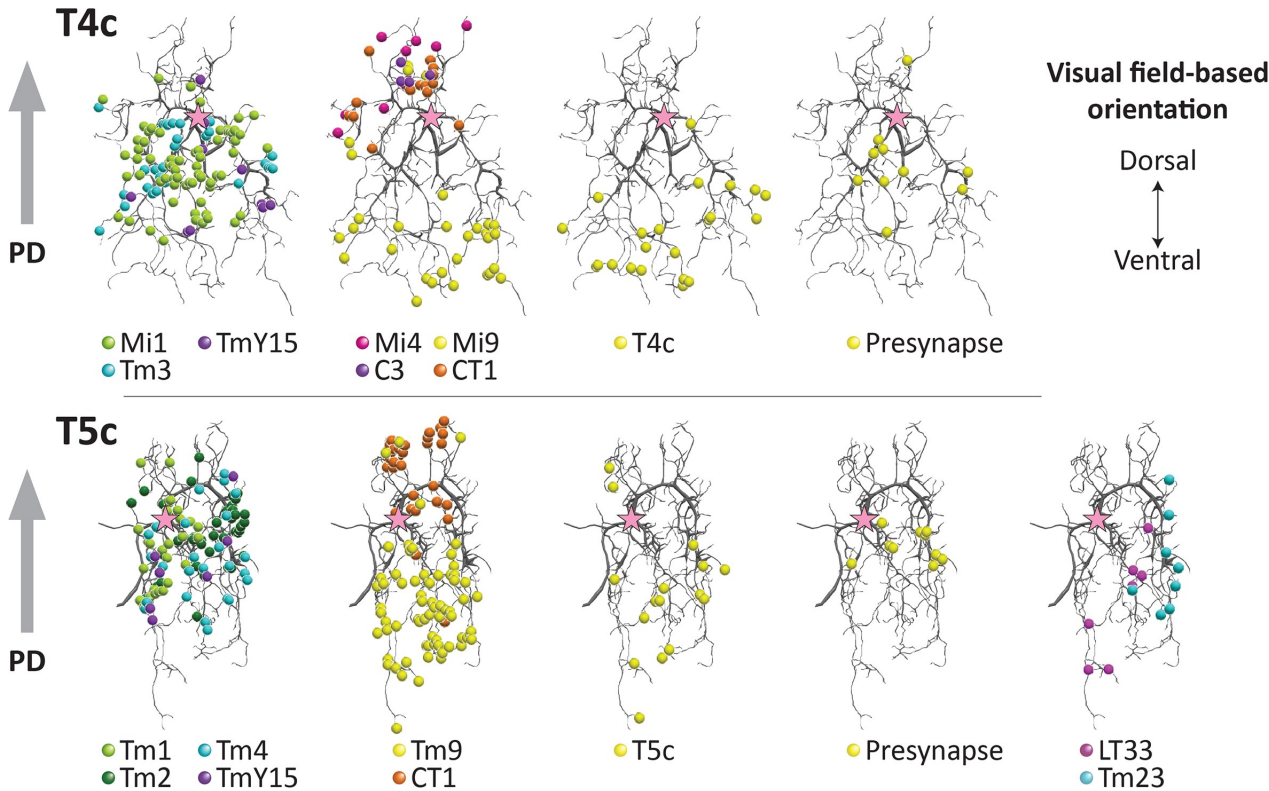


Figure 5: t4t5inputsynapses

Most of these input elements have been characterised physiologically (Arenz2017; Serbe2016; Strother2017; Meier2019; Borst2020). None of these cells were found to be direction-selective. Hence, we can conclude that T4 and T5 are the first elementary motion detector found in the ON and OFF pathway respectively, and thus represents an important processing stage where direction is computed.

## 1.6 NEURAL ALGORITHM UNDERLYING DIRECTION SELECTIVITY

The underlying mechanisms generating direction selectivity and the neural correlates implementing these mechanisms have not been yet fully understood. Classically two opposing models have been proposed for implementation of direction selectivity. Both these model use two input lines, where one of the input line has been asymmetrically delayed compared to the other, which is then followed by a non-linear interaction. The Hassenstein-Reichardt (HR) model proposes a Preferred Direction (PD) enhancement : the signal on the preferred side is delayed and is subsequently amplified using multiplication of the signal from the other input line [Figure](**Hassenstein1956**). The Barlow-Levick (BL) detector however, proposes a Null Direction (ND) suppression : the signal on the null side is delayed and divides the signal from the other input resulting in suppression (**Barlow1965**) . **Haag2016a** used apparent motion stimuli to show that both the mechanisms i.e. PD enhancement and ND suppression is used by T4 and T5 cell to produce a direction selective response. In our **manuscript1** - (**Haag2017**), we showed that all four subtypes of T4 and T5 indeed uses both PD enhancement and ND suppression to produce direction selective responses. Therefore, a new model combining both PD enhancement on the preferred side and ND suppression on the null side was proposed. The next important task now is to identify neural correlates implementing these mechanisms.

The model requires a fast input at the center, slow input providing excitation on the preferred side and slow input providing suppression on the null side. Interestingly, from the anatomical and functional characterization of input data we have discussed earlier, we could predict the input neurons for T4 providing these three kind of inputs. Mi1 is a fast neuron providing input at the central part of dendrite, thus a candidate for central fast input. Mi9 is a slow neuron providing input on the preferred side of the dendrite, hence a candidate for slow excitatory input. Mi4, C3 and CT1 are slow neurons providing input on the null side of the dendrite. In **manuscript2** we have expressed GtACR or ReaChr to silence or activate input neurons respectively. Simultaneously, we express GCaMP in the downstream T4c/T5c neurons. These experiments together help us understand the functional contribution of each of these input neurons to direction selective signals in T4.



# 2 | PUBLICATIONS

## 2.1 A COMMON DIRECTIONAL TUNING MECHANISM OF *Drosophila* MOTION-SENSING NEURONS IN THE ON AND IN THE OFF PATHWAY

**ABSTRACT** In the fruit fly optic lobe, T<sub>4</sub> and T<sub>5</sub> cells represent the first direction-selective neurons, with T<sub>4</sub> cells responding selectively to moving brightness increments (ON) and T<sub>5</sub> cells to brightness decrements (OFF). Both T<sub>4</sub> and T<sub>5</sub> cells comprise four subtypes with directional tuning to one of the four cardinal directions. We had previously found that upward-sensitive T<sub>4</sub> cells implement both preferred direction enhancement and null direction suppression (Haag et al., 2016). Here, we asked whether this mechanism generalizes to OFF-selective T<sub>5</sub> cells and to all four subtypes of both cell classes. We found that all four subtypes of both T<sub>4</sub> and T<sub>5</sub> cells implement both mechanisms, that is preferred direction enhancement and null direction inhibition, on opposing sides of their receptive fields. This gives rise to the high degree of direction selectivity observed in both T<sub>4</sub> and T<sub>5</sub> cells within each subpopulation.

**AUTHORS** Juergen Haag, **Abhishek Mishra** and Alexander Borst

**CONTRIBUTIONS** Juergen Haag, Conceptualization, Data curation, Software, Investigation, Visualization, Writing, review and editing; Abhishek Mishra, Investigation; Alexander Borst, Conceptualization, Funding acquisition, Writing original draft, Project administration, Writing, review and editing





# A common directional tuning mechanism of *Drosophila* motion-sensing neurons in the ON and in the OFF pathway

Juergen Haag\*, Abhishek Mishra, Alexander Borst

Max-Planck-Institute of Neurobiology, Martinsried, Germany

**Abstract** In the fruit fly optic lobe, T4 and T5 cells represent the first direction-selective neurons, with T4 cells responding selectively to moving brightness increments (ON) and T5 cells to brightness decrements (OFF). Both T4 and T5 cells comprise four subtypes with directional tuning to one of the four cardinal directions. We had previously found that upward-sensitive T4 cells implement both preferred direction enhancement and null direction suppression (Haag et al., 2016). Here, we asked whether this mechanism generalizes to OFF-selective T5 cells and to all four subtypes of both cell classes. We found that all four subtypes of both T4 and T5 cells implement both mechanisms, that is preferred direction enhancement and null direction inhibition, on opposing sides of their receptive fields. This gives rise to the high degree of direction selectivity observed in both T4 and T5 cells within each subpopulation.

DOI: <https://doi.org/10.7554/eLife.29044.001>

## Introduction

The direction of visual motion is crucial for fundamental behaviors such as mate detection, prey capture, predator avoidance and visual navigation. This important visual cue, however, is not explicitly encoded at the output of a single photoreceptor but rather has to be computed by subsequent neural circuits. In order to extract local, directional information from moving images, mainly two competing algorithmic models of motion detectors have been proposed (*Figure 1a,b*). Both models implement a delay-and-compare mechanism where two input signals from neighboring image pixels interact in a nonlinear way after one of them has been delayed with respect to the other. This leads to an output that is larger for motion along one, the so-called ‘preferred’ direction than for the opposite, the so-called ‘null’ direction. Both models differ, however, by the type of non-linearity employed and the location of the delay. In the Hassenstein-Reichardt detector (*Figure 1a*), the delay is on the preferred side, that is where a preferred direction stimulus is entering the receptive field of the detector, and the non-linearity is excitatory. This leads to an enhancement of signals moving in the preferred direction (*Hassenstein and Reichardt, 1956*). In the Barlow-Levick detector (*Figure 1b*), the delay is on the null side, that is where a null direction stimulus is entering the receptive field of the detector, and the nonlinearity is inhibitory. This leads to a suppression of signals moving in the null direction (*Barlow and Levick, 1965*). While the predictions of both models concerning the responses to smooth grating motion are identical, apparent motion stimuli lend themselves well to discriminate between them (*Egelhaaf and Borst, 1992; Eichner et al., 2011*). Instead of moving an object smoothly across the image plane, an apparent motion stimulus consists of a bright or dark bar or spot that is abruptly jumped from one location to an adjacent one. Comparing the responses of directional neurons to the sequence with the sum of the responses to each individual stimulus presentation (‘linear expectation’) allows one to calculate the nonlinear response component as the difference between the sequence response and the linear expectation. If this nonlinear response component is positive for sequences along the preferred direction, and zero for

\*For correspondence:  
haag@neuro.mpg.de

Competing interest: See  
page 13

Funding: See page 12

Received: 30 May 2017

Accepted: 21 August 2017

Published: 22 August 2017

Reviewing editor: Fred Rieke,  
Howard Hughes Medical  
Institute, University of  
Washington, United States

© Copyright Haag et al. This  
article is distributed under the  
terms of the [Creative Commons  
Attribution License](#), which  
permits unrestricted use and  
redistribution provided that the  
original author and source are  
credited.

sequences along the null direction, a preferred direction enhancement is at work, supporting the Hassenstein-Reichardt model (*Figure 1a*). If the nonlinear response component is zero for sequences along the preferred direction and negative for sequences along the null direction, a null direction suppression is at work, supporting the Barlow-Levick model (*Figure 1b*). In the following, we will apply this approach in order to investigate which of the two mechanisms is at work in primary motion-sensitive neurons of the fruit fly *Drosophila*.

In *Drosophila*, visual signals are processed in the optic lobe, a brain area comprised of the lamina, medulla, lobula, and lobula plate, each arranged in a columnar, retinotopic fashion (for review, see: *Borst, 2014; Behnia and Desplan, 2015*). In striking parallel to the vertebrate retina (*Borst and Helmstaedter, 2015*), the direction of visual motion is computed within the optic lobe separately in parallel ON and OFF motion pathways (*Joesch et al., 2010; Reiff et al., 2010; Eichner et al., 2011; Joesch et al., 2013*). Anatomically, these two pathways split at the level of the lamina (*Bausenwein et al., 1992; Rister et al., 2007*) and lead, via a set of various intrinsic medulla and transmedulla interneurons, onto the dendrites of T4 and T5 cells, respectively. First described by Golgi staining (*Cajal and Sanchez, 1915; Strausfeld, 1976; Strausfeld and Lee, 1991; Fischbach and Dittrich, 1989*), T4 cells extend their dendrites in the most proximal layer of the medulla, while the dendrites of T5 cells are located in the inner-most layer of the lobula. There exist generally four T4 and 4 T5 cells per column (*Mauss et al., 2014*). The four subtypes of T4 cells respond selectively to brightness increments moving along one of the four cardinal directions, the four subtypes of T5 cells selectively to brightness decrements moving along the same four cardinal directions as T4 cells (*Maisak et al., 2013*). According to their preferred direction, T4 and T5 cells project into one of the four lobula plate layers (layer 1, most frontal: front-to-back; layer 2: back-to-front; layer 3: upward; layer 4, most posterior: downward; *Maisak et al., 2013*). There, T4 and T5 cells provide direct excitatory cholinergic input onto the dendrites of wide-field, motion-sensitive tangential cells as well as onto glutamatergic lobula plate interneurons that inhibit wide-field tangential cells in the adjacent layer (*Mauss et al., 2014; Mauss et al., 2015*). Through this circuit arrangement, lobula plate tangential cells depolarize to motion in their preferred direction (PD) and hyperpolarize in response to motion in the opposite or null direction (ND) (*Joesch et al., 2008; Schnell et al., 2010*). With T4 and T5 cells blocked, tangential cells lose all their direction selectivity (*Schnell et al., 2012*) and flies become completely motion-blind (*Bahl et al., 2013; Schilling and Borst, 2015*). This suggests that T4 and T5 cells are the elementary motion detectors and carry all directional information in the fly brain. Electrophysiological (*Behnia et al., 2014*), optical voltage (*Yang et al., 2016*) and Calcium recordings (*Meier et al., 2014; Serbe et al., 2016; Arenz et al., 2017; Strother et al., 2014; Strother et al., 2017*) from presynaptic medulla neurons revealed that none of them is directionally selective. Therefore, T4 and T5 cells are the first neurons in the visual processing chain that respond to visual motion in a direction selective manner.

Previous studies analyzed the mechanism underlying direction selectivity in T4 and T5 cells, yet arrived at different conclusions. Using apparent motion stimuli, one study found preferred direction enhancement to account for directional responses in T4 cells (*Fisher et al., 2015*). For T5 cells, the authors reported both enhancement for preferred and suppression for null direction sequences, but attributed the latter to circuit adaptation and not to the mechanism generating direction selectivity. The authors concluded that the dominant interaction producing direction selective responses in both T4 and T5 cells is a nonlinear signal amplification (*Fisher et al., 2015*). This conflicts with another report where spatio-temporal receptive fields of T5 cells were measured using white noise stimulation and reverse correlation. Based on ON and OFF subfields tilted in the space-time plane, T5 cells were concluded to incorporate both preferred direction enhancement and null direction suppression (*Leong et al., 2016*). This interpretation, however, suffers from a possible confusion of ON and OFF receptive subfields of T5 input neurons with the mechanism generating direction selectivity within T5 cells themselves. Addressing the same question, we recently applied apparent motion stimuli to one class of T4 cells that have upward as their preferred direction and, thus, project to layer 3 of the lobula plate. Using a telescopic stimulation technique to place the stimulus precisely onto the hexagonal lattice of the fly's eye (*Kirschfeld, 1967; Braitenberg, 1967; Franceschini, 1975; Schuling et al., 1989*), layer 3 T4 cells turned out to implement both mechanisms within different

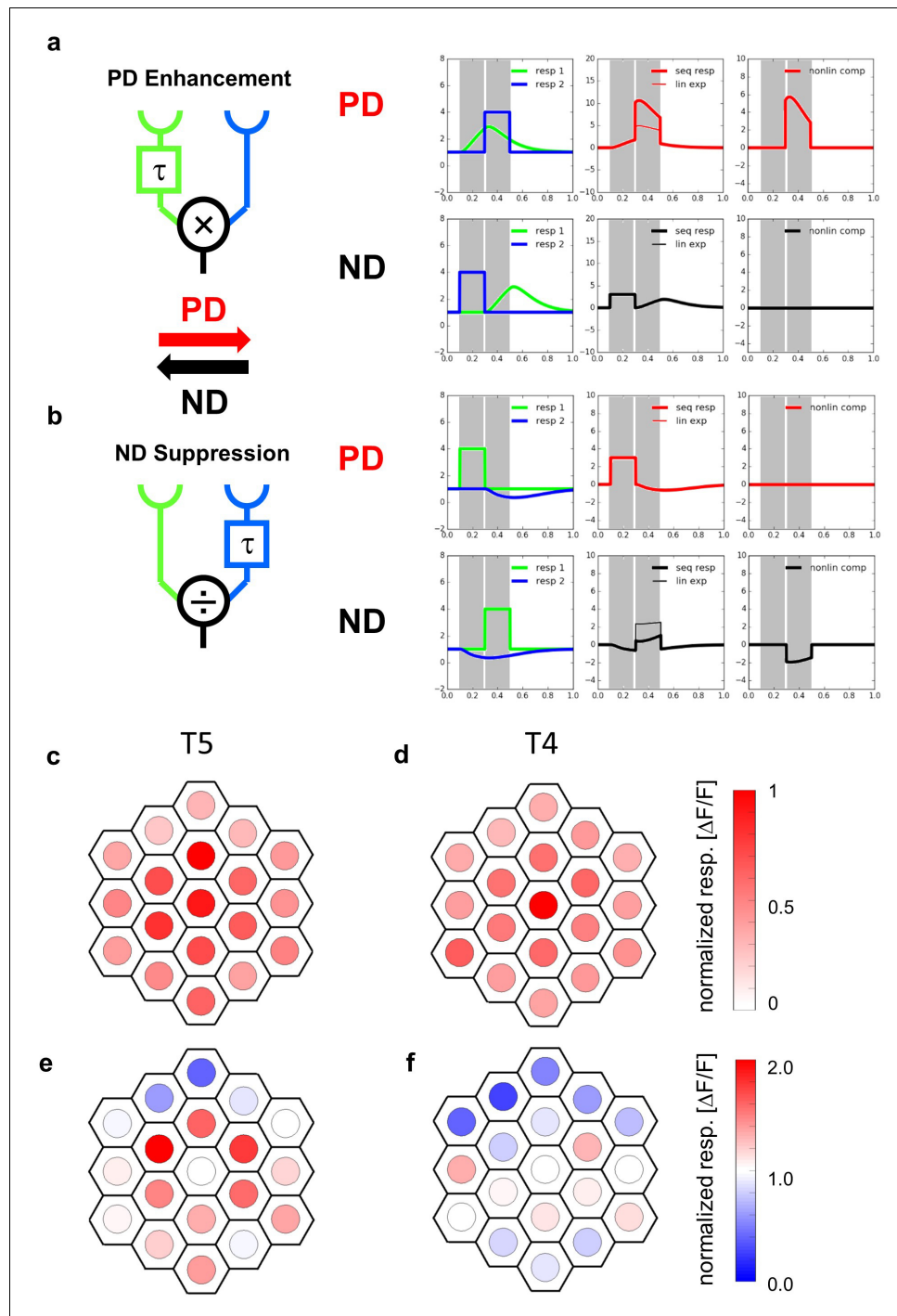


**Figure 1.** Receptive fields and responses to apparent motion stimuli of T5-cells. (a) The Hassenstein-Reichardt model incorporates PD enhancement only, realized by a multiplication. Left: Responses to individual light pulses ('Flicker') delivered at the two different positions. The responses are shifted according to the stimulus sequence used for the subsequent apparent motion stimuli. Middle: Responses of the model to apparent motion stimuli in preferred (upper row) and null direction (lower row, thick line = measured response, thin line = linear expectation, that is sum of responses to the single

Figure 1 continued on next page

**Figure 1 continued**

light pulses). Right: Nonlinear response component defined as the difference between measured response and linear expectation. (b) same as (a) but for a Barlow-Levick model. This model incorporates ND-suppression only, realized by a division. (c) Average responses of five T5 cells to flicker stimuli (stimulus size: 5 degree) delivered to different optical columns. In order to average the responses of different flies, the response patterns were aligned and normalized with respect to the maximum response (central column) and shown in a false color code. (d) Same as (c) but for T4-cells. Data represent the mean of 10 T4-cells from 10 flies (from [Haag et al., 2016](#)). (e) Responses of T5 cells to stimuli presented to the central column and simultaneously to one of the columns of the two surrounding rings. As in c, the responses of different flies were aligned with respect to the column eliciting the maximum response when stimulated individually and normalized to it. Depending on the location, simultaneous stimulation of a second column led to either a suppressed (blue colors) or an enhanced (red colors) response compared to the exclusive stimulation of the central column. The suppression is stronger on the null side of the T5 cells. Data represent the mean of 6 T5 cells from 6 different flies. (f) Same as e) but for T4-cells. Data represent the mean of T4-cells from 8 flies (from [Haag et al., 2016](#)).

DOI: <https://doi.org/10.7554/eLife.29044.002>

The following figure supplements are available for figure 1:

**Figure supplement 1.**

DOI: <https://doi.org/10.7554/eLife.29044.003>

**Figure supplement 2.** Responses of T4-cells and T5 cells to stimuli presented to the central column and simultaneously to one of the columns of the two surrounding rings.

DOI: <https://doi.org/10.7554/eLife.29044.004>

parts of their receptive field ([Haag et al., 2016](#)): While preferred direction enhancement was found to be dominant within the ventral part of the receptive field, a null direction suppression was significant in the dorsal part of their receptive field ([Haag et al., 2016](#)).

To resolve the conflicting evidences mentioned above and to test whether T5 cells are using the same or a different mechanism to compute the direction of motion as do T4 cells, we used the same strategy as in our previous account ([Haag et al., 2016](#)) and applied it to investigate the mechanism underlying direction selective responses of both T4 and T5 cells of all four directional tuning subtypes.

## Results

In a first set of experiments, we used the same driver line as in our previous study ([Haag et al., 2016](#)) expressing the Calcium indicator GCaMP6m ([Chen et al., 2013](#)) in both T4 and T5 cells projecting to layer 3 of the lobula plate and, hence, having upward motion as their preferred direction. Since T5 cells are known to be OFF sensitive, we used dark spots on a bright background projected onto the raster of optical columns via a telescope to stimulate the cells and recorded the fluorescence changes in the lobula plate. We started by measuring the flicker responses of T5 cells to optical stimulation of 19 individual columns, forming two rings surrounding a central column. In [Figure 1c](#), the responses of five T5 cells were averaged and are shown in false color code overlaid on the columnar raster. T5 cells responded maximally to the stimulation of the central column, with about 50–100% amplitude to stimulation of the surrounding columns and about 20–50% to the next outer ring. An individual example trace and statistical evaluation of the responses are shown in [Figure 1—figure supplement 1](#). Compared to T4 cells ([Figure 1d](#), data replotted from [Haag et al., 2016](#)), the receptive field of T5 cells turned out to be broader with a somewhat stronger sensitivity within the surrounding columns. To explore spatial interactions within the receptive field of T5-cells, we stimulated the central column, simultaneously with one of surrounding columns. The results ([Figure 1e](#)) indicate a strong suppression of the response in the dorsal part of the receptive field compared to when the central column was stimulated alone, similar to what was found previously for T4 cells ([Figure 1f](#), data replotted from [Haag et al., 2016](#)).

Experiments performed on layer 3 T4 cells with apparent motion stimuli revealed different mechanisms of direction selectivity in different parts of the receptive field ([Haag et al., 2016](#)): Two-pulse apparent motion stimuli in the dorsal part of the receptive field led to a null direction suppression, apparent motion stimuli in the ventral part evoked preferred direction enhancement. We asked whether we could find this spatial arrangement of null direction suppression and preferred direction enhancement in T5 cells as well. In order to measure that, we presented OFF stimuli to four neighboring columns along the dorsal-ventral axis ([Figure 2a,b](#)). The columns were chosen in relation to

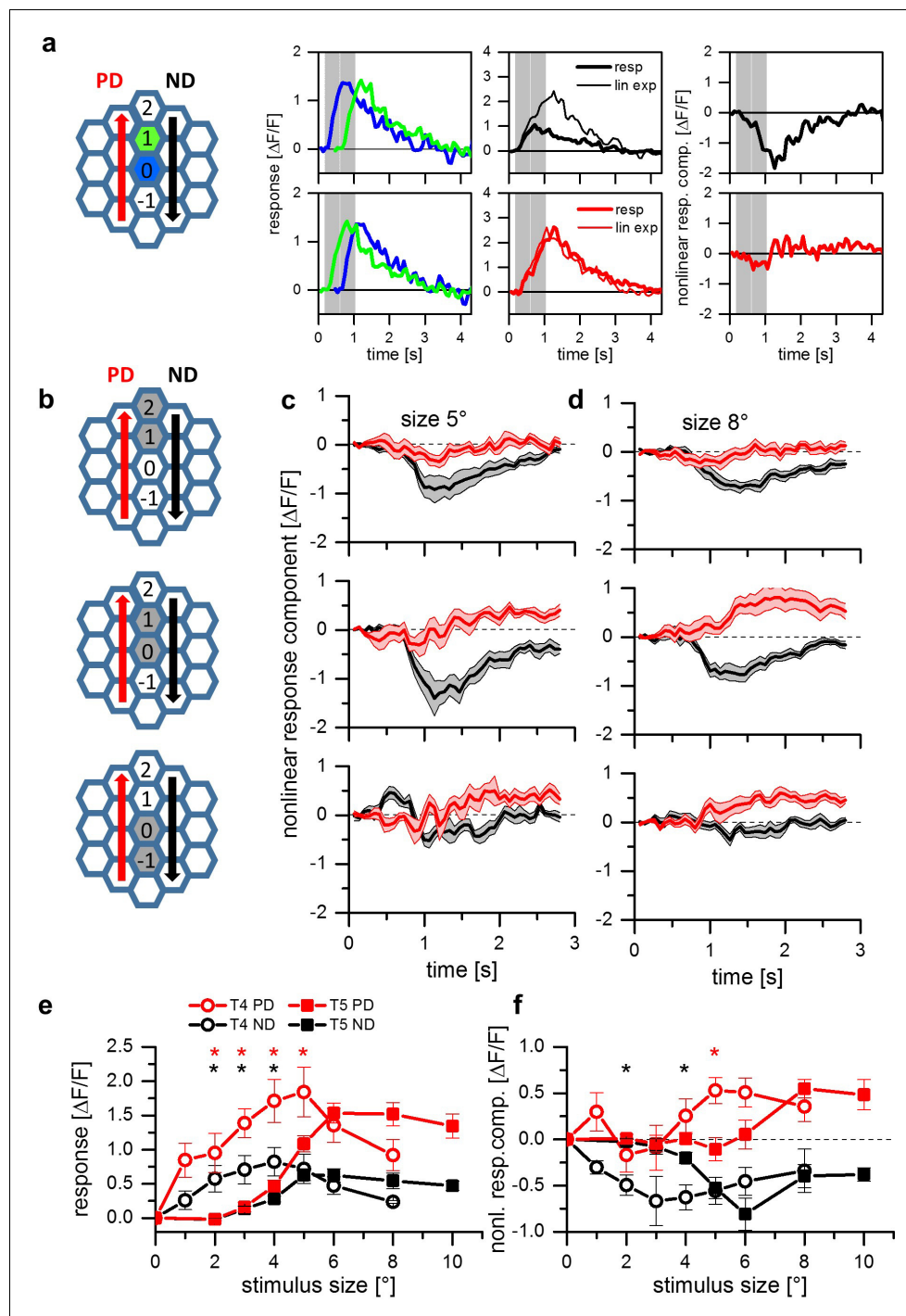


**Figure 2.** Apparent motion stimuli between adjacent cartridges. (a) Response of a single T5 cell recorded in a single sweep to two-step apparent motion stimuli. The schematic to the left shows the position of the two stimuli (blue and green shading). Left: Responses to individual light pulses ('Flicker') delivered at the two different positions. The responses are shifted in time according to the stimulus sequence used for the subsequent apparent motion stimuli. Middle: Responses of T5 to apparent motion stimuli in preferred and null direction (thick line = measured response, thin

## Figure 2 continued

line = linear expectation, that is sum of responses to the single light pulses). Right: Nonlinear response component defined as the difference between measured sequence response and linear expectation. The responses are the mean obtained from  $n = 3$  stimulus repetitions. (b) Two-step apparent motion stimuli were shown at three different position in the receptive field of T5 cells. The stimulus consisted of light off pulses positioned on one column for 472 ms, immediately followed by a light off pulse for 472 ms to the upper, neighboring cartridge. The same stimuli were repeated along the opposite direction. (c) Nonlinear response component, that is the difference between sequence response and the sum of the responses to the individual pulses, as a function of time for a stimulus size of 5 degree. Apparent motion stimuli delivered to the upper two cartridges resulted in a null direction suppression and no preferred direction enhancement. Apparent motion stimuli in the lower cartridges did not lead to a deviation from the linear expectation. For all three stimuli no preferred direction enhancement could be found. Data represent the mean  $\pm$  SEM in 6 T5-cells measured in 6 different flies. (d) Same as d, but with a stimulus size of 8 degree. In contrast to the results for a smaller stimulus size, we found preferred direction enhancement for stimulation of the lower and the central pair of columns. Data shows the mean  $\pm$  SEM in 10 T5-cells measured in 8 different flies. (e) Responses of T4 (open circles) and T5 cells (closed squares) to apparent motion stimuli in preferred (red colors) and null direction (black colors) between the two central columns 0 and 1. Compared to the responses of T4, T5 responses to two-pulse sequences along the preferred (PD) and the null (ND) direction are shifted to larger stimulus sizes. Data represent the mean values  $\pm$  SEM of 10 T5 cells measured in 5 flies and of 7 T4 cells in 4 different flies, respectively. Black asterisks represent statistically significant (*t*-test,  $p$ -value  $< 0.05$ ) differences for null-direction responses of T4-cells and T5-cells, red asterisks for preferred direction responses. (f) Nonlinear response components of T4 and T5 cells. Same dataset as in **Figure 1e**.

DOI: <https://doi.org/10.7554/eLife.29044.005>

the column that elicited the strongest response in each cell (central column 0). We then tested T5 cells with two consecutive light OFF pulses of 472 ms duration in immediate succession. Each light pulse was positioned on one of two neighboring columns resulting in three stimulus sequences (**Figure 2b**). To extract the nonlinear response component, we subtracted the sum of the responses to the individual stimuli from the response to the apparent motion sequence. Example traces from an individual experiment stimulating columns 0 and 1 are shown in **Figure 2a**. Using the same spot diameter as in our previous account, that is 5 degree, we found null direction suppression for stimulation of the central (column 0 and 1) and the dorsal (column 1 and 2) pairs, and only a slight, if any, sign of preferred direction enhancement for stimulation of the ventral pair (column -1 and 0) (**Figure 2c**). This changed when we enlarged the spot size from 5 to 8 degree. Now, in addition to null direction suppression for the central and dorsal stimulus pairs, preferred direction enhancement for the ventral and central stimulus pairs was observed (**Figure 2d**). This result mirrors our previous finding for T4 cells where both null direction suppression and preferred direction enhancement was found to account for direction selectivity (Haag et al., 2016). In further agreement with T4 cells, these two mechanisms are spatially separated, with null direction suppression on the null and preferred direction enhancement on the preferred side of the receptive field (Haag et al., 2016).

The above experiments indicate a different dependence of null direction suppression and preferred direction enhancement on the diameter of the stimulus spot in T5 cells. To measure this dependence in a gradual way, we again used apparent motion stimuli and varied the size of the stimuli from 1 to 10 degree. Since stimuli centered on the central column pair (0 and 1) resulted in both types of nonlinearity (**Figure 2d**, middle graph), we presented apparent motion stimuli with different stimulus sizes to these central columns only. To compare the results of T5 cells with the ones of T4 cells, the stimulus set consisted of either bright pulses on a dark background (for T4 cells) or dark pulses on a bright background (for T5 cells). **Figure 2e** shows the responses of T4 (circle symbols) and T5 (square symbols) to apparent motion stimuli as a function of the stimulus size for preferred (PD, red traces) and null (ND, black traces) direction sequences. For both directions of motion, T4 cells respond to smaller stimuli than T5 cells. The strongest response in T4 can be found for stimulus sizes of 4 to 5 deg. For stimulus sizes beyond these values, the responses of T4 cells decline. In contrast, T5 cells only start responding at these stimulus sizes and plateau for larger values. When instead of the response the nonlinear response component is plotted as a function of the stimulus size (**Figure 2f**, same symbol and color code as in **Figure 2e**), both preferred direction enhancement and null direction suppression become apparent, with both curves shifted to larger stimulus sizes for T5 cells. Furthermore, for both cell types, null direction suppression peaks at smaller stimulus sizes than preferred direction enhancement.

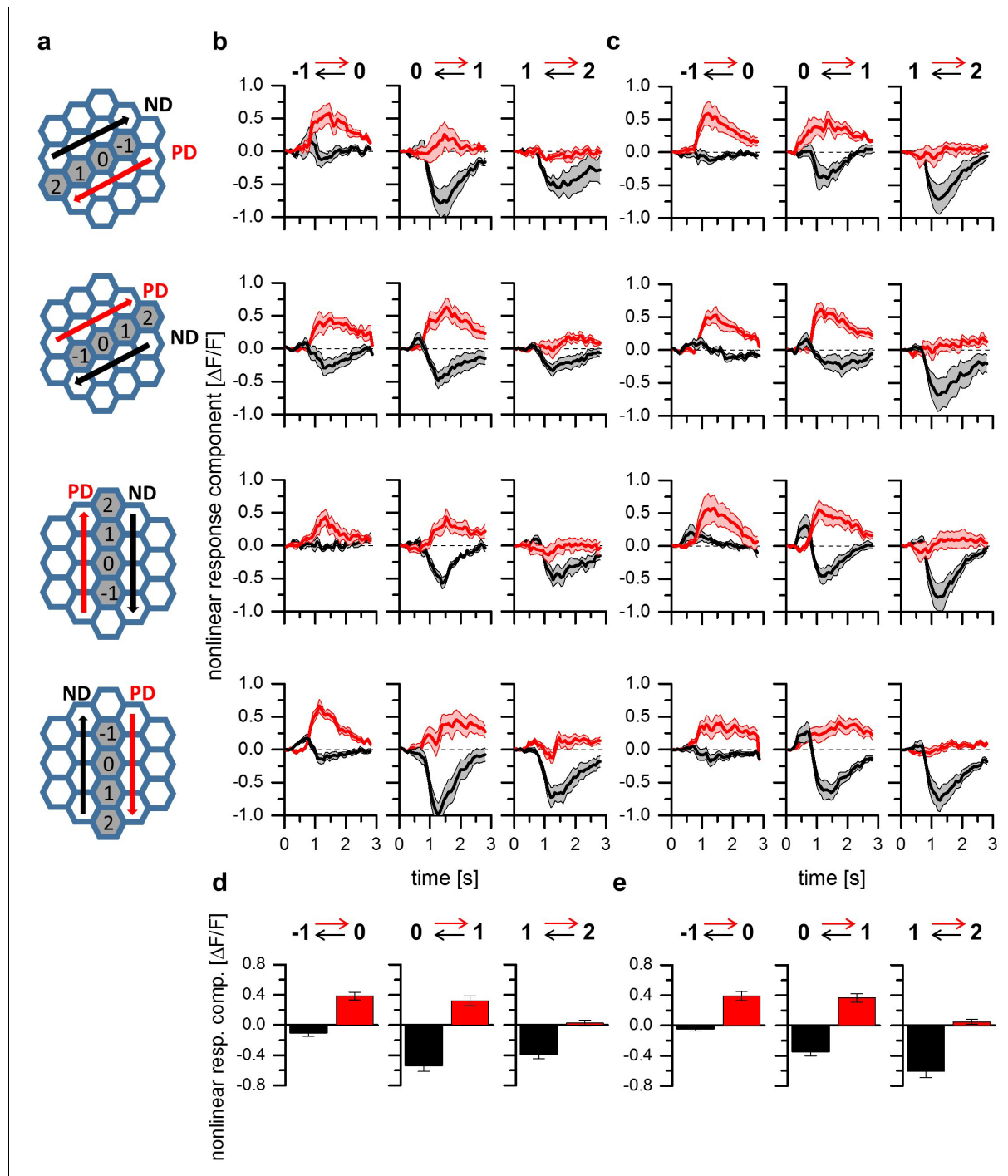
The results presented so far point towards a common mechanism for T4 and T5 cells underlying direction selectivity. However, the experiments on T4 and T5 cells were confined to those that terminate in layer 3 of the lobula plate. In order to investigate whether the properties described above

generalize to T4 and T5 cells of all four tuning categories, we next used a fly line expressing GCaMP5 in T4 and T5 cells projecting to all four layers. Similar to the experiments shown in **Figure 2c and d**, two-step apparent motion stimuli consisting of ON-ON pulses of 5 degree diameter for T4 cells as well of OFF-OFF pulses of 8 degree diameter for T5 cells were presented in three adjacent pairs of columns aligned to the column that elicited the strongest flicker response (**Figure 3a**). As before, the stimulus protocol consisted in the presentation of individual stimulus pulses for the calculation of the linear expectation as well as in the presentation of the two-pulse sequences, to measure the sequence response. From the latter, the linear expectation was subtracted to obtain the nonlinear response component. The time traces of these nonlinear response components are shown in **Figure 3b and c**. For T4 (**Figure 3b**) and T5 (**Figure 3c**) cells projecting to all layers, we found both preferred direction and null direction suppression, with a spatial separation that follows the same pattern: on the preferred side of the receptive field, a clear preferred direction enhancement was observed without any null direction suppression (**Figure 3b and c**, left column). In the center of the receptive field, both preferred direction enhancement and null direction suppression prevailed (**Figure 3b and c**, center column). On the null side of the receptive field, only null direction suppression was detectable (**Figure 3b and c**, right column). To investigate possible differences between T4 and T5 cells and between cells with different directional tuning, we performed a 3-way ANOVA test. Choosing a significance level of  $p=0.05$ , no significant differences were found, neither between T4 and T5 cells, nor between the neurons projecting to the four different layers. In **Figure 3d** (T4 cells) and **3e** (T5 cells), the nonlinear response components are shown as averaged between 1 and 2 s of the time courses shown above, as well as averaged across the cells from all four layers. On these data, two-sided t-tests were performed between T4 and T5 cell responses for each individual stimulus condition. Choosing again a significance level of  $p=0.05$ , no differences were found between T4 and T5 cell responses for 5 out of 6 stimulus conditions. Only the response amplitude of T4 cells to null direction stimulus sequences from column 2 to 1 was found to be significantly smaller than the respective value of T5 cells.

The results from apparent motion experiments reported so far suggest a common directional tuning mechanism for T4 and T5 cells for all cardinal directions. One, thus, would expect identical high degrees of direction selectivity in response to moving gratings mechanism within the different layers of the lobula plate. To test this directly, we used the same fly line as above expressing in both T4 and T5 cells of all four layers and presented grating motion along all four cardinal directions on a screen. For each pixel, we first calculated the vector sum of the responses and represented the vector angle in false color. The resulting image from one example fly is shown in **Figure 4a**. Clearly, the preferred direction is extremely homogeneous with little variation within each layer. We repeated such experiments in five different flies and determined the distribution of all preferred directions obtained from the whole data set. The histogram (**Figure 4b**) reveals exactly four sharp peaks separated by 90 degrees, corresponding to the preferred directions of T4 and T5 cells within each of the four layers. This transition from the hexagonal coordinates of the fly eye to Cartesian coordinates is likely to occur on the dendrites of T4 and T5 cells by their sampling from appropriately grouped columns ([Takemura et al., 2017](#)). From the same data set, we calculated a direction selectivity index for each pixel within each layer as the difference of the responses to preferred and null direction, divided by the sum of the responses. We then determined the mean direction selectivity for each layer from each fly and averaged the resulting values across the different experiments. The results reveal an extremely high degree of direction selectivity of about 0.8 that is almost identical within each layer (**Figure 4c**). To measure direction selectivity separately for T4 and T5 cells, we stimulated the flies with ON and OFF edges instead of gratings and obtained similar values of about 0.8 on average (**Figure 4d**).

## Discussion

Having analyzed the mechanisms underlying direction selectivity of all four subtypes of both T4 and T5 cells, we found a common scheme that pertains to all of these cells: regardless of the directional tuning and the contrast preference for ON or OFF stimuli, elementary motion-sensitive neurons in *Drosophila* implement a preferred direction enhancement on the preferred side and a null direction suppression of input signals on the null side of their receptive field.



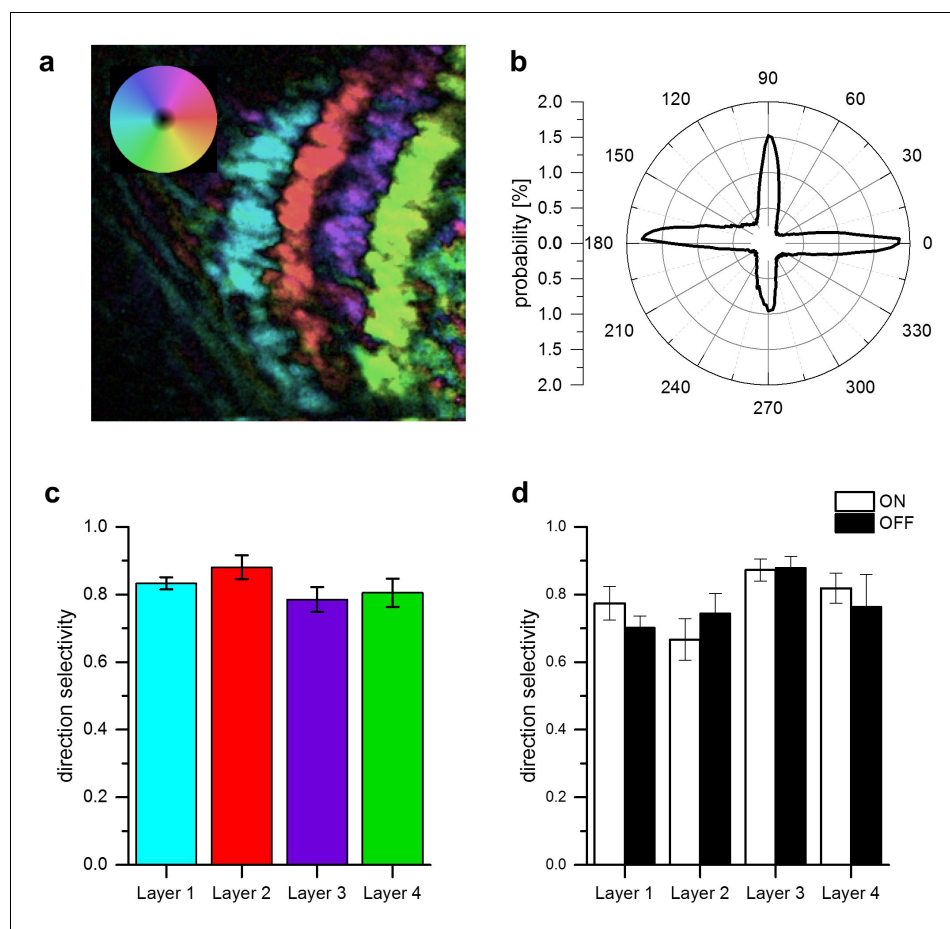
**Figure 3.** A common mechanism for direction selectivity in all four subtypes of T4 and T5 cells. **(a)** Pictograms indicating the stimulus positions and the preferred and null-direction of the respective layer. **(b)** Nonlinear response components of T4-cells to apparent motion stimuli in different layers of the lobula plate. For T4 cells projecting to all four layers, preferred direction enhancement and null direction suppression are found to be spatially distributed within the receptive field such that enhancement is found on the preferred side while suppression is predominant on the null side of the Figure 3 continued on next page

Figure 3 continued

receptive field. Data represent the mean  $\pm$  SEM of 6, 8, 7 and 9 T4 cells (from layer 1–4). (c) Nonlinear response components of T5 cells to apparent motion stimuli in different layers of the lobula plate. Data represent the mean  $\pm$  SEM of 8, 5, 6 and 13 T5 cells (from layer 1–4).

DOI: <https://doi.org/10.7554/eLife.29044.006>

ON and OFF pathways seemed to have adapted to the asymmetry of luminance distributions found in the real world. Consequently, functional differences between ON and OFF pathways have been described in the mammalian retina and in flies as well (Ratliff et al., 2010; Clark et al., 2014; Baden et al., 2016; Leonhardt et al., 2016). In fly motion vision, our finding of a common mechanism for T4 and T5 cells suggests the above mentioned asymmetries to rely on quantitative instead of qualitative differences, such as different time-constants used by the ON and the OFF pathway (Leonhardt et al., 2016; Arenz et al., 2017). One difference between T4 and T5 cells found in this



**Figure 4.** Directional tuning and selectivity of T4 and T5 cells. (a) Example of directional tuning to grating motion as determined by the vector sum of responses to grating motion along four cardinal directions. All neurons within each layer have almost identical preferred directions. (b) Histogram of preferred directions within all four layers. Clear peaks appear at the four cardinal directions. Data were obtained from 5 different flies. (c) Direction selectivity within each layer, as defined by the difference between the preferred and null direction responses, divided by the sum. Data represent the mean  $\pm$  SEM obtained from 5 flies (same data set as in b). (d) Same as c, but flies were stimulated by ON and OFF edges, respectively. Data represent the mean  $\pm$  SEM obtained from 3 flies.

DOI: <https://doi.org/10.7554/eLife.29044.007>

study relates to the dependence of the directional motion signal on the spot size in the apparent motion paradigm (**Figure 2e,f**). Given a half-width of the photoreceptor acceptance angle of approximately 5 degree in *Drosophila* (Götz, 1965), any stimulus is spatially low-pass filtered by a Gaussian with 5 degree full width at half maximum. Accordingly, enlarging the spot size will have two different effects: first, it will lead to an increasing peak intensity at the column where the stimulus spot is centered on, and second, it will lead to an increasing activation of neurons in neighboring columns. Which of these two effects is responsible for the higher threshold of T5 cells compared to T4 cells, and whether the sensitivity difference is in the input neurons or in T4/T5 cells themselves, cannot be decided by the present study.

In any case, our finding readily explains the high degree of direction selectivity found already at the processing stage where direction-selective signals first arise: neither a signal enhancement for preferred direction sequences nor a signal suppression for null direction sequences by itself would lead to such a strong direction selectivity as observed experimentally with large signals for preferred direction motion and zero responses for null direction motion (Maisak et al., 2013; Fisher et al., 2015). In analogy to the results presented for layer 3 T4 cells (Figure 5 in Haag et al., 2016), the responses of all T4 and T5 cells can be captured in algorithmic terms by a common mechanism, using a delayed, low-pass filtered input on the preferred side enhancing a fast, central input, with the result being suppressed by again a low-pass filtered input on the null side.

At the next processing stage, that is at the level of lobula plate tangential cells, the signals of oppositely tuned T4 and T5 cells become subtracted via inhibitory lobula plate interneurons (Mauss et al., 2015). This process, in a way, replicates the action of null direction suppression implemented on the dendrites of T4 and T5 cells. Since both mechanisms, that is the combination of preferred direction enhancement and null direction suppression on the dendrites of T4 and T5 cells as well as the subtraction of oppositely tuned T4 and T5 cells on the dendrites of tangential cells lead to high degree of direction selectivity at the output of the system, one might ask about the functional advantage of such a dual strategy. This question can be answered by either blocking null direction suppression on the T4/T5 cells dendrite or blocking the inhibitory lobula plate interneurons. The latter experiment has indeed been done, and the results revealed a loss of flow-field specificity of the tangential cells, due to the lack of inhibition caused by the non-matching part of the optic flow field (Mauss et al., 2015). For the converse situation, no experimental data exist so far and one has to rely on computer simulations (Haag et al., 2016, Figure 5). They suggest that a high direction selectivity is retained in tangential cells. This high degree of direction selectivity, however, rests on the relatively small differences between large, but poorly tuned signals and, thus, would be highly prone to noise. Improving the direction-tuning already at the level of T4 and T5 cells by the additional null-direction suppression should, therefore, increase the system's robustness to noise.

Our results open the door to the next level question about its neural implementation. Here, a recent connectomic study identified the major interneurons providing synaptic input to T4 cells as well as their placement on the dendrite (Takemura et al., 2017). Takemura and colleagues describe 4 columnar cell types, that is Mi1, Mi4, Mi9 and Tm3 as the major input elements to T4 cells, in addition to columnar cell types C3, TmY15, a wide-field neuron CT1 and other T4 cells with identical preferred direction. Columnar input neurons contact the T4 cell dendrite in a way that depends on the direction tuning subtype: while Mi9 synapses are clustered on the preferred side of the dendrite, Mi1 and Tm3 synapse on the central part and Mi4 are found predominantly on the null side. Most interestingly, the dynamic response properties of these different types of T4 input neurons match their position on the dendrite to suggest a specific function in the detector model discussed above: Mi9 and Mi4 indeed exhibit the temporal low-pass properties postulated for the inputs on the preferred and the null side, while Mi1 and Tm3 display fast band-pass properties needed for the central input (Arenz et al., 2017). This proposed correspondence needs to be tested by blocking individual input cell types and measuring the resulting effect on direction selectivity in T4 cells. Specifically, one would expect to abolish preferred direction enhancement when blocking Mi9, while blocking Mi4 should lead to a loss of null direction suppression. It is, however, important to stress that the effect of such blocking experiments is expected to be quite specific and directly observable only in directional responses of T4 cells: due to further network processing involving a subtraction of T4 cell signals with opposite directional tuning at the level of tangential cells (see previous paragraph, and Mauss et al., 2015), the effect might be far more subtle when downstream cells or behavior are used as a read-out (Strother et al., 2017). Nevertheless, blocking the central inputs Mi1 and Tm3

while recording from tangential cells revealed that Mi1 cells are absolutely essential for proper functioning of the ON pathway under all stimulus conditions tested, while blocking Tm3 only led to a loss of sensitivity for high edge velocities (Ammer et al., 2015). With respect to the polarity of the synapses of the various T4 input neurons, the correspondence outlined above predicts that Mi1 and Tm3 are excitatory while Mi4 should be inhibitory. In line with this, recent studies suggest a cholinergic phenotype in Mi1 and Tm3 (Pankova and Borst, 2017; Takemura et al., 2017) and a GABAergic one in Mi4 (Takemura et al., 2017). Seemingly in contrast to an enhancing action of Mi9 postulated above, this cell was found to be OFF sensitive (Arenz et al., 2017). However, Mi9 turned out to be immune-positive for the vesicular Glutamate reporter VGluT (Takemura et al., 2017). Together with the inhibitory action of Glutamate via the GluCl channel, well documented for other neurons of the Drosophila CNS (Liu and Wilson, 2013; Mauss et al., 2014; Mauss et al., 2015), this raises the possibility that Mi9 enhances the input from Mi1 and Tm3 onto T4 by a release from inhibition.

As for T4 cells, the major input neurons to T5 cells were identified by an EM study (Shinomiya et al., 2014). There, trans-medulla neurons Tm1, Tm2, Tm4, and Tm9 were found to make up for about 80% of all input synapses to T5 cell dendrites. However, the exact placement of the different inputs on the dendrite and, hence, the relative position of their receptive fields could not be determined by this report. As for their dynamic properties, only one of the cell types, Tm9, reveals low-pass characteristics, while all others (Tm1, Tm2 and Tm4) can be described as band-pass filters with different time-constants (Meier et al., 2014; Serbe et al., 2016; Arenz et al., 2017). In analogy of the arrangement of input neurons of T4 cells, Arenz et al., 2017 found that placing the two slowest cells (Tm1 and Tm9) on the outer arms and the fast Tm2 cell on the central arm of the three-input detector gives rise to a motion detector that fits real T5 cells both with respect to their high degree of direction selectivity and their temporal tuning optimum. Since, in contrast to T4 cells, the position of these interneurons on the dendrite of T5 cells is less well known so far, no prediction can be made whether blocking of Tm1 should lead to a loss of preferred direction enhancement and blocking of Tm9 to a loss of null direction suppression, or the other way round. Therefore, as is the case with T4 cells, further experiments are needed to determine which cell is playing which role in the functional context of preferred direction enhancement and null direction inhibition determined by the present study.

In summary, thus, we have found a common, uniform mechanism of direction selectivity for T4 and T5 cells that consists of combination of preferred direction enhancement and null direction suppression in different location of their receptive field, precisely related to their directional tuning. Mapping the different input neurons to T4 and T5 cells to their specific function in this context represents the next step of the analysis. The major challenge for future experiments will then consist in understanding the biophysical mechanisms underlying enhancement and suppression. Here, different ideas have been discussed in the past (Torre and Poggio, 1978; Koch and Poggio, 1992; Gabbiani et al., 2002), and the different thresholds for preferred direction enhancement and null direction suppression described above might be an important result to decide between the various possibilities. These can now be tested at the molecular level using genome editing techniques available in *Drosophila* (Venken et al., 2011; Zhang et al., 2014; Fisher et al., 2017; Pankova and Borst, 2017).

## Materials and methods

### Flies

(*Drosophila melanogaster*) were raised at 25°C and 60% humidity on a 12 hr light/12 hr dark cycle on standard cornmeal agar medium. For calcium imaging of T5 cells, flies were used expressing the genetically-encoded calcium indicator GCaMP6m (Chen et al., 2013) in T4/T5 neurons with axon terminals predominantly in layer 3 of the lobula plate ( $w^-$ ; Sp/cyo; VT50384-lexA, lexAop-GCaMP6m/TM6b). For the imaging experiments of T4 and T5 cells in the four layers of the lobula plate we used flies expressing the calcium indicator GCaMP5 in both T4 and T5 cells in all layers of the lobula plate ( $w^-$ ;  $+/+$ ; UAS-GCaMP5, R42F06-GAL4/UAS-GCaMP5, R42F06-GAL4).

## Calcium imaging

Fly surgery was performed, and the neuronal activity was measured from the left optical lobe on a custom-built 2-photon microscope (Denk et al., 1990) as previously described (Haag et al., 2016). Images were acquired at a resolution of  $64 \times 64$  pixels and at a frame rate of 15 Hz with the ScanImage software (Pologruto et al., 2003) in Matlab.

## Optical stimulation

Stimulation with a telescopic stimulus device was similar to that used in our previous study (Haag et al., 2016). For the experiments shown in **Figure 4**, a regular stimulus display was used as described in (Arenz et al., 2017). The gratings had a spatial wavelength of 30 deg, a contrast of 100%, a mean luminance of  $34 \text{ cd/m}^2$  and was moving along one of the four cardinal directions at 30 deg/sec.

## Experimental protocol

In order to discriminate between T4 and T5 cells we stimulated single optical columns with bright pulses on a dark background. The cells were selected based on their response to light-on stimuli. While T4 cells respond to the onset of a light pulse, the T5 cells respond to the light-off. For the experiments the stimuli consisted either of dark pulses on a bright background (T5 cells) or bright pulses on a dark background (T4 cells). The pulses had a duration of 472 ms. At each position, three stimulus presentations were delivered. The resulting responses were averaged and the peak of the averaged response was taken. Apparent motion stimuli consisted of consecutive light stimuli to two neighboring cartridges. The second stimulus was presented right after the first turned off, resulting in a delay from onset to onset of 472 ms.

## Data analysis

was performed offline using custom-written routines in Matlab. Regions of interests (ROIs) were selected by hand of the lobula plate. Time courses of relative fluorescence changes ( $\Delta F/F$ ) were calculated from the raw imaging sequence. Responses to the stimulus were baseline-subtracted, averaged across repetitions, and quantified as the peak responses over the stimulus epochs. Those responses were averaged across experiments. Where indicated, responses were normalized to the maximum average response before averaging. For the apparent motion experiments, non-linear response components were calculated as the differences of the time-courses of the responses to the apparent motion stimuli and the sum of the appropriately time-shifted responses to flicker stimuli at the corresponding positions.

## Acknowledgements

We thank Georg Ammer, Alexander Arenz and Alex Mauss for critically reading the ms. This work was supported by the Max-Planck-Society and the Deutsche Forschungsgemeinschaft (SFB 870).

---

## Additional information

### Competing interests

Alexander Borst: Reviewing editor, eLife. The other authors declare that no competing interests exist.

### Funding

Funder	Grant reference number	Author
Max-Planck-Gesellschaft		Juergen Haag Abhishek Mishra Alexander Borst
Deutsche Forschungsgemeinschaft	SFB 870	Juergen Haag Abhishek Mishra Alexander Borst

---

The funders had no role in study design, data collection and interpretation, or the decision to submit the work for publication.

#### Author contributions

Juergen Haag, Conceptualization, Data curation, Software, Investigation, Visualization, Writing—review and editing; Abhishek Mishra, Investigation; Alexander Borst, Conceptualization, Funding acquisition, Writing—original draft, Project administration, Writing—review and editing

#### Author ORCIDs

Juergen Haag  <https://orcid.org/0000-0002-6535-0103>  
Abhishek Mishra  <http://orcid.org/0000-0002-1933-1251>  
Alexander Borst  <http://orcid.org/0000-0001-5537-8973>

#### Decision letter and Author response

Decision letter <https://doi.org/10.7554/eLife.29044.010>  
Author response <https://doi.org/10.7554/eLife.29044.011>

## Additional files

### Supplementary files

- Transparent reporting form  
DOI: <https://doi.org/10.7554/eLife.29044.008>

## References

- Ammer G, Leonhardt A, Bahl A, Dickson BJ, Borst A. 2015. Functional Specialization of Neural Input Elements to the Drosophila ON Motion Detector. *Current Biology* **25**:2247–2253. DOI: <https://doi.org/10.1016/j.cub.2015.07.014>, PMID: 26234212
- Arenz A, Drews MS, Richter FG, Ammer G, Borst A. 2017. The Temporal Tuning of the Drosophila Motion Detectors Is Determined by the Dynamics of Their Input Elements. *Current Biology* **27**:929–944. DOI: <https://doi.org/10.1016/j.cub.2017.01.051>, PMID: 28343964
- Baden T, Berens P, Franke K, Román Rosón M, Bethge M, Euler T. 2016. The functional diversity of retinal ganglion cells in the mouse. *Nature* **529**:345–350. DOI: <https://doi.org/10.1038/nature16468>, PMID: 26735013
- Bahl A, Ammer G, Schilling T, Borst A. 2013. Object tracking in motion-blind flies. *Nature Neuroscience* **16**:730–738. DOI: <https://doi.org/10.1038/nn.3386>, PMID: 23624513
- Barlow HB, Levick WR. 1965. The mechanism of directionally selective units in rabbit's retina. *The Journal of Physiology* **178**:477–504. DOI: <https://doi.org/10.1113/jphysiol.1965.sp007638>, PMID: 5827909
- Bausenwein B, Dittrich AP, Fischbach KF. 1992. The optic lobe of Drosophila melanogaster. II. Sorting of retinotopic pathways in the medulla. *Cell and Tissue Research* **267**:17–28. PMID: 1735111
- Behnia R, Clark DA, Carter AG, Clandinin TR, Desplan C. 2014. Processing properties of ON and OFF pathways for Drosophila motion detection. *Nature* **512**:427–430. DOI: <https://doi.org/10.1038/nature13427>, PMID: 25043016
- Behnia R, Desplan C. 2015. Visual circuits in flies: beginning to see the whole picture. *Current Opinion in Neurobiology* **34**:125–132. DOI: <https://doi.org/10.1016/j.conb.2015.03.010>, PMID: 25881091
- Borst A, Helmstaedter M. 2015. Common circuit design in fly and mammalian motion vision. *Nature Neuroscience* **18**:1067–1076. DOI: <https://doi.org/10.1038/nn.4050>, PMID: 26120965
- Borst A. 2014. Fly visual course control: behaviour, algorithms and circuits. *Nature Reviews Neuroscience* **15**:590–599. DOI: <https://doi.org/10.1038/nrn3799>, PMID: 25116140
- Braitenberg V. 1967. Patterns of projection in the visual system of the fly. I. Retina-lamina projections. *Experimental Brain Research* **3**:271–298. DOI: <https://doi.org/10.1007/BF00235589>, PMID: 6030825
- Cajal SR, Sanchez D. 1915. *Contribucion Al Conocimiento De Los Centros Nerviosos De Los Insectos*. Madrid: Imprenta de Hijos de Nicholas Moja.
- Chen TW, Wardill TJ, Sun Y, Pulver SR, Renninger SL, Baohan A, Schreiter ER, Kerr RA, Orger MB, Jayaraman V, Looger LL, Svoboda K, Kim DS. 2013. Ultrasensitive fluorescent proteins for imaging neuronal activity. *Nature* **499**:295–300. DOI: <https://doi.org/10.1038/nature12354>, PMID: 2386828
- Clark DA, Fitzgerald JE, Ales JM, Gohl DM, Silies MA, Norcia AM, Clandinin TR. 2014. Flies and humans share a motion estimation strategy that exploits natural scene statistics. *Nature Neuroscience* **17**:296–303. DOI: <https://doi.org/10.1038/nn.3600>, PMID: 24390225
- Denk W, Strickler JH, Webb WW. 1990. Two-photon laser scanning fluorescence microscopy. *Science* **248**:73–76. DOI: <https://doi.org/10.1126/science.2321027>, PMID: 2321027

- Egelhaaf M, Borst A. 1992. Are there separate ON and OFF channels in fly motion vision? *Visual Neuroscience* **8**: 151–164. DOI: <https://doi.org/10.1017/S0952523800009317>, PMID: 1558827
- Eichner H, Joesch M, Schnell B, Reiff DF, Borst A. 2011. Internal structure of the fly elementary motion detector. *Neuron* **70**:1155–1164. DOI: <https://doi.org/10.1016/j.neuron.2011.03.028>, PMID: 21689601
- Fischbach K-F, Dittrich APM. 1989. The optic lobe of *Drosophila melanogaster*. I. A Golgi analysis of wild-type structure. *Cell and Tissue Research* **258**:441–475. DOI: <https://doi.org/10.1007/BF00218858>
- Fisher YE, Silies M, Clandinin TR. 2015. Orientation Selectivity Sharpens Motion Detection in Drosophila. *Neuron* **88**:390–402. DOI: <https://doi.org/10.1016/j.neuron.2015.09.033>, PMID: 26456048
- Fisher YE, Yang HH, Isaacman-Beck J, Xie M, Gohl DM, Clandinin TR. 2017. FlpStop, a tool for conditional gene control in Drosophila. *eLife* **6**:e22279. DOI: <https://doi.org/10.7554/eLife.22279>, PMID: 28211790
- Franceschini N. 1975. Sampling of the visual environment by the compound eye of the fly: fundamentals and applications. In: Snyder (Ed). *Photoreceptor Optics*. p. 98–125.
- Gabbiani F, Krapp HG, Koch C, Laurent G. 2002. Multiplicative computation in a visual neuron sensitive to looming. *Nature* **420**:320–324. DOI: <https://doi.org/10.1038/nature01190>, PMID: 12447440
- Götz KG. 1965. Die optischen Übertragungseigenschaften der Komplexaugen von Drosophila. *Kybernetik* **2**:215–221. DOI: <https://doi.org/10.1007/BF00306417>
- Haag J, Arenz A, Serbe E, Gabbiani F, Borst A. 2016. Complementary mechanisms create direction selectivity in the fly. *eLife* **5**:e17421. DOI: <https://doi.org/10.7554/eLife.17421>, PMID: 27502554
- Hassenstein B, Reichardt W. 1956. Systemtheoretische analyse der zeit-, reihenfolgen- und vorzeichenauswertung bei der bewegungsperzeption des rüsselkäfers Chlorophanus. *Zeitschrift Für Naturforschung B* **11**:513–524.
- Joesch M, Plett J, Borst A, Reiff DF. 2008. Response properties of motion-sensitive visual interneurons in the lobula plate of *Drosophila melanogaster*. *Current Biology* **18**:368–374. DOI: <https://doi.org/10.1016/j.cub.2008.02.022>, PMID: 18328703
- Joesch M, Schnell B, Raghu SV, Reiff DF, Borst A. 2010. ON and OFF pathways in *Drosophila* motion vision. *Nature* **468**:300–304. DOI: <https://doi.org/10.1038/nature09545>, PMID: 21068841
- Joesch M, Weber F, Eichner H, Borst A. 2013. Functional specialization of parallel motion detection circuits in the fly. *Journal of Neuroscience* **33**:902–905. DOI: <https://doi.org/10.1523/JNEUROSCI.3374-12.2013>, PMID: 23325229
- Kirschfeld K. 1967. Die projekion der optischen umwelt auf das raster der rhabdomere im komplexauge von *Musca*. *Experimental Brain Research* **3**:248–270. DOI: <https://doi.org/10.1007/BF00235588>
- Koch C, Poggio T. 1992. Multiplying with synapses and neurons. In: , McKenna T, Davis J, Zornetzer SF (Eds). *And Single Neuron Computation*. Boston, Sand Diego, new Ork, London, Sydney, Tokyo, Toronto: Academic Press. p. 315–345.
- Leong JC, Esch JJ, Poole B, Ganguli S, Clandinin TR. 2016. Direction Selectivity in *Drosophila* Emerges from Preferred-Direction Enhancement and Null-Direction Suppression. *Journal of Neuroscience* **36**:8078–8092. DOI: <https://doi.org/10.1523/JNEUROSCI.1272-16.2016>, PMID: 27488629
- Leonhardt A, Ammer G, Meier M, Serbe E, Bahl A, Borst A. 2016. Asymmetry of *Drosophila* ON and OFF motion detectors enhances real-world velocity estimation. *Nature Neuroscience* **19**:706–715. DOI: <https://doi.org/10.1038/nn.4262>, PMID: 26928063
- Liu WW, Wilson RI. 2013. Glutamate is an inhibitory neurotransmitter in the *Drosophila* olfactory system. *PNAS* **110**:10294–10299. DOI: <https://doi.org/10.1073/pnas.1220560110>, PMID: 23729809
- Maisak MS, Haag J, Ammer G, Serbe E, Meier M, Leonhardt A, Schilling T, Bahl A, Rubin GM, Nern A, Dickson BJ, Reiff DF, Hopp E, Borst A. 2013. A directional tuning map of *Drosophila* elementary motion detectors. *Nature* **500**:212–216. DOI: <https://doi.org/10.1038/nature12320>, PMID: 23925246
- Mauss AS, Meier M, Serbe E, Borst A. 2014. Optogenetic and pharmacologic dissection of feedforward inhibition in *Drosophila* motion vision. *Journal of Neuroscience* **34**:2254–2263. DOI: <https://doi.org/10.1523/JNEUROSCI.3938-13.2014>, PMID: 24501364
- Mauss AS, Pankova K, Arenz A, Nern A, Rubin GM, Borst A. 2015. Neural circuit to integrate opposing motions in the visual field. *Cell* **162**:351–362. DOI: <https://doi.org/10.1016/j.cell.2015.06.035>, PMID: 26186189
- Meier M, Serbe E, Maisak MS, Haag J, Dickson BJ, Borst A. 2014. Neural circuit components of the *Drosophila* OFF motion vision pathway. *Current Biology* **24**:385–392. DOI: <https://doi.org/10.1016/j.cub.2014.01.006>, PMID: 24508173
- Pankova K, Borst A. 2017. Transgenic line for the identification of cholinergic release sites in *Drosophila melanogaster*. *The Journal of Experimental Biology* **220**:1405–1410. DOI: <https://doi.org/10.1242/jeb.149369>, PMID: 28167805
- Pologruto TA, Sabatini BL, Svoboda K. 2003. ScanImage: flexible software for operating laser scanning microscopes. *Biomedical Engineering Online* **2**:13. DOI: <https://doi.org/10.1186/1475-925X-2-13>, PMID: 12801419
- Ratliff CP, Borghuis BG, Kao YH, Sterling P, Balasubramanian V. 2010. Retina is structured to process an excess of darkness in natural scenes. *PNAS* **107**:17368–17373. DOI: <https://doi.org/10.1073/pnas.1005846107>, PMID: 20855627
- Reiff DF, Plett J, Mank M, Griesbeck O, Borst A. 2010. Visualizing retinotopic half-wave rectified input to the motion detection circuitry of *Drosophila*. *Nature Neuroscience* **13**:973–978. DOI: <https://doi.org/10.1038/nn.2595>, PMID: 20622873

- Rister J, Pauls D, Schnell B, Ting CY, Lee CH, Sinakevitch I, Morante J, Strausfeld NJ, Ito K, Heisenberg M. 2007. Dissection of the peripheral motion channel in the visual system of *Drosophila melanogaster*. *Neuron* **56**:155–170. DOI: <https://doi.org/10.1016/j.neuron.2007.09.014>, PMID: 17920022
- Schilling T, Borst A. 2015. Local motion detectors are required for the computation of expansion flow-fields. *Biology Open* **4**:1105–1108. DOI: <https://doi.org/10.1242/bio.012690>, PMID: 26231626
- Schnell B, Joesch M, Forstner F, Raghu SV, Otsuna H, Ito K, Borst A, Reiff DF. 2010. Processing of horizontal optic flow in three visual interneurons of the *Drosophila* brain. *Journal of Neurophysiology* **103**:1646–1657. DOI: <https://doi.org/10.1152/jn.00950.2009>, PMID: 20089816
- Schnell B, Raghu SV, Nern A, Borst A. 2012. Columnar cells necessary for motion responses of wide-field visual interneurons in *Drosophila*. *Journal of Comparative Physiology A* **198**:389–395. DOI: <https://doi.org/10.1007/s00359-012-0716-3>, PMID: 22411431
- Schulung FH, Mastebroek HAK, Bult R, Lenting BPM. 1989. Properties of elementary movement detectors in the fly *Calliphora erythrocephala*. *Journal of Comparative Physiology A* **165**:179–192. DOI: <https://doi.org/10.1007/BF00619192>
- Serbe E, Meier M, Leonhardt A, Borst A. 2016. Comprehensive characterization of the major presynaptic elements to the *Drosophila* OFF motion detector. *Neuron* **89**:829–841. DOI: <https://doi.org/10.1016/j.neuron.2016.01.006>, PMID: 26853306
- Shinomiya K, Karuppudurai T, Lin TY, Lu Z, Lee CH, Meinertzhagen IA. 2014. Candidate neural substrates for off-edge motion detection in *Drosophila*. *Current Biology* **24**:1062–1070. DOI: <https://doi.org/10.1016/j.cub.2014.03.051>, PMID: 24768048
- Strausfeld N. 1976. *Atlas of an Insect Brain*. Heidelberg, New York, Berlin: Springer Verlag.
- Strausfeld NJ, Lee JK. 1991. Neuronal basis for parallel visual processing in the fly. *Visual Neuroscience* **7**:13–33. DOI: <https://doi.org/10.1017/S095252380010919>, PMID: 1931797
- Strother JA, Nern A, Reiser MB. 2014. Direct observation of ON and OFF pathways in the *Drosophila* visual system. *Current Biology* **24**:976–983. DOI: <https://doi.org/10.1016/j.cub.2014.03.017>, PMID: 24704075
- Strother JA, Wu ST, Wong AM, Nern A, Rogers EM, Le JO, Rubin GM, Reiser MB. 2017. The Emergence of Directional Selectivity in the Visual Motion Pathway of *Drosophila*. *Neuron* **94**:168–182. DOI: <https://doi.org/10.1016/j.neuron.2017.03.010>, PMID: 28384470
- Takemura SY, Nern A, Chklovskii DB, Scheffer LK, Rubin GM, Meinertzhagen IA. 2017. The comprehensive connectome of a neural substrate for 'ON' motion detection in *Drosophila*. *eLife* **6**:e24394. DOI: <https://doi.org/10.7554/eLife.24394>, PMID: 28432786
- Torre V, Poggio T. 1978. A synaptic mechanism possibly underlying directional selectivity to motion. *Proceedings of the Royal Society B: Biological Sciences* **202**:409–416. DOI: <https://doi.org/10.1098/rspb.1978.0075>
- Venken KJ, Schulze KL, Haelterman NA, Pan H, He Y, Evans-Holm M, Carlson JW, Levis RW, Spradling AC, Hoskins RA, Bellen HJ. 2011. MiMIC: a highly versatile transposon insertion resource for engineering *Drosophila melanogaster* genes. *Nature Methods* **8**:737–743. DOI: <https://doi.org/10.1038/nmeth.1662>, PMID: 21985007
- Yang HH, St-Pierre F, Sun X, Ding X, Lin MZ, Clandinin TR. 2016. Subcellular imaging of voltage and calcium signals reveals neural processing in vivo. *Cell* **166**:245–257. DOI: <https://doi.org/10.1016/j.cell.2016.05.031>, PMID: 27264607
- Zhang X, Koolhaas WH, Schnorrer F. 2014. A Versatile Two-Step CRISPR- and RMCE-Based Strategy for Efficient Genome Engineering in *Drosophila*. *G3: Genes|Genomes|Genetics* **4**:2409–2418. DOI: <https://doi.org/10.1534/g3.114.013979>



## 2.2 VOLTAGE TO CALCIUM TRANSFORMATION ENHANCES DIRECTION SELECTIVITY IN *Drosophila* T4 NEURONS

**ABSTRACT** A critical step in neural information processing is the transformation of membrane voltage into calcium signals leading to transmitter release. However, the effect of voltage to calcium transformation on neural responses to different sensory stimuli is not well understood. Here, we use *in vivo* two-photon imaging of genetically encoded voltage and calcium indicators, Arclight and GCaMP6f respectively, to measure responses in *Drosophila* direction-selective T4 neurons. Comparison between Arclight and GCaMP6f signals revealed calcium signals to have a significantly higher direction selectivity compared to voltage signals. Using these recordings we build a model which transforms T4 voltage responses to calcium responses. The model reproduces experimentally measured calcium responses across different visual stimuli using different temporal filtering steps and a stationary non-linearity. These findings provide a mechanistic underpinning of the voltage-to-calcium transformation and show how this processing step, in addition to synaptic mechanisms on the dendrites of T4 cells, enhances direction selectivity in the output signal of T4 neurons.

**AUTHORS** Abhishek Mishra, Alexander Borst, and Juergen Haag

**CONTRIBUTIONS** Abhishek Mishra, Conceptualization, Investigation, Data curation, Software, Visualization, Writing original draft, review and editing; Juergen Haag, Conceptualization, Data curation, Software, Investigation, review and editing; Alexander Borst, Conceptualization, Funding acquisition, Project administration, Review and editing



# <sup>1</sup> Voltage to Calcium Transformation <sup>2</sup> Enhances Direction Selectivity in <sup>3</sup> *Drosophila* T4 neurons

<sup>4</sup> Abhishek Mishra<sup>1,2</sup>, Alexander Borst<sup>1,2</sup>, Juergen Haag<sup>1</sup>

<sup>5</sup> <sup>1</sup>Max Planck Institute for Biological Intelligence (in foundation), Martinsried, Germany;

<sup>6</sup> <sup>2</sup>Graduate School of Systemic Neurosciences, LMU Munich, Martinsried, Germany

<sup>7</sup> 

---

<sup>8</sup> **Abstract** A critical step in neural information processing is the transformation of membrane  
9 voltage into calcium signals leading to transmitter release. However, the effect of voltage to calcium  
10 transformation on neural responses to different sensory stimuli is not well understood. Here, we  
11 use *in vivo* two-photon imaging of genetically encoded voltage and calcium indicators, Arclight and  
12 GCaMP6f respectively, to measure responses in *Drosophila* direction-selective T4 neurons.  
13 Comparison between Arclight and GCaMP6f signals revealed calcium signals to have a significantly  
14 higher direction selectivity compared to voltage signals. Using these recordings we build a model  
15 which transforms T4 voltage responses to calcium responses. The model reproduces  
16 experimentally measured calcium responses across different visual stimuli using different temporal  
17 filtering steps and a stationary non-linearity. These findings provide a mechanistic underpinning of  
18 the voltage-to-calcium transformation and show how this processing step, in addition to synaptic  
19 mechanisms on the dendrites of T4 cells, enhances direction selectivity in the output signal of T4  
20 neurons.

<sup>21</sup> 

---

**Introduction**

<sup>22</sup> In order to guide animal behavior, neurons perform a wide range of computations. Neurons encode  
23 information via graded changes in membrane potential or action potential frequency. Mostly they  
24 communicate via chemical synapses which requires the release of neurotransmitters. When the  
25 presynaptic membrane is sufficiently depolarized, voltage-gated calcium channels open and allow  
26  $Ca^{2+}$  to enter the cell (Luo 2020). Calcium entry leads to the fusion of synaptic vesicles with the  
27 membrane and release of neurotransmitter molecules into the synaptic cleft (Chapman 2002).  
28 As neurotransmitters diffuse across the synaptic cleft, they bind to receptors in the postsynaptic  
29 membrane, causing postsynaptic neuron to depolarize or hyperpolarize, passing the information  
30 from pre to postsynaptic neurons (Di Maio 2008). Voltage to calcium transformation therefore  
31 represents one crucial step in neural information processing and neural computation.

<sup>32</sup> A classic example of neural computation is how *Drosophila* neurons compute the direction  
33 of visual motion (Borst *et al.* 2020). In *Drosophila*, visual information is processed in parallel ON  
34 (contrast increments) and OFF (contrast decrements) pathways (Joesch *et al.* 2010; Eichner *et al.*  
35 2011). Direction selectivity emerges three synapses downstream of photoreceptors, in T4 and T5  
36 for ON and OFF pathways respectively. Four subtypes of T4 and T5 cells exist, each responding  
37 selectively to one of the four cardinal directions (Maisak *et al.* 2013). Amazingly, right at the  
38 first stage where direction selectivity emerges, T4 and T5 cells exhibit a high degree of direction  
39 selectivity, with no responses to null direction stimuli. This statement is, however, based on calcium

41 recordings. Whole-cell patch clamp recordings show a somewhat different picture: While preferred  
42 direction stimuli also lead to large membrane depolarizations, edges or gratings moving along  
43 the null directions elicit smaller but significant responses as well (Wienecke *et al.* 2018; Groschner  
44 *et al.* 2022). This hints to an additional processing step where voltage signals are transformed  
45 into calcium signals that increases direction selectivity of the cells. In order to study this step  
46 systematically, we recorded both voltage and calcium signals in response to a large stimulus set  
47 that includes gratings and edges moving along various directions at different speeds and contrasts.  
48 Using these data, we build a model that captures the transformation from voltage to calcium by a  
49 few linear and non-linear processing steps.

## 50 Results

51 We first expressed the genetically encoded calcium indicator GCaMP6f (Chen *et al.* 2013) in T4 cells  
52 projecting to layer 3 of the lobula plate. These cells have upward motion as their preferred direction  
53 (PD) and downward motion as their null direction (ND). We also expressed the genetically encoded  
54 voltage indicator Arclight (Jin *et al.* 2012) using the same driver line. Arclight's fluorescence decreases  
55 with membrane depolarization and increases with membrane hyperpolarization. To compare the  
56 voltage and calcium signals, we recorded the neural activity in T4c cells dendrites in medulla layer 10  
57 in response to the same set of stimuli using 2-photon microscopy (Denk *et al.* 1990). The complete  
58 stimuli set included square-wave gratings of 30° spatial wavelength moving in 12 different directions,  
59 and ON edges moving in PD and ND, at four different speeds ( $15^{\circ}s^{-1}$ ,  $30^{\circ}s^{-1}$ ,  $60^{\circ}s^{-1}$ ,  $120^{\circ}s^{-1}$ ) and four  
60 different contrasts (10%, 20%, 50%, 100%).

61 In a first set of experiments, we measured the voltage and calcium signals in response to  
62 gratings moving in PD and ND at four different speeds (figure 1A). As the grating stimuli consists  
63 of alternate bright and dark bars moving in a certain direction, there was a modulation in the  
64 Arclight (black traces) and GCaMP6f (red traces) responses to it. The GCaMP6f responses showed  
65 modulations only for slower speeds, while Arclight responses revealed modulations also for faster  
66 speeds. The response amplitudes were much higher for GCaMP6f ( $\approx 2.0\Delta F/F$ ) compared to Arclight  
67 ( $\approx -0.06\Delta F/F$ ). The peak responses (maximum  $\Delta F/F$ ) decreased with increasing stimulus speed  
68 both for GCaMP6f and Arclight (figure 1B). To understand if voltage to calcium transformation  
69 affects direction selectivity in T4 cells, we compared the responses to gratings moving in PD and  
70 ND. GCaMP6f responses in ND were negligible compared to its responses in PD, while for Arclight  
71 responses in ND were quite visible. We quantified the direction selectivity using a direction selectivity  
72 index (DSI) calculated as the difference of the peak responses to preferred and null direction, divided  
73 by the sum of the peak responses (Materials and Methods equation (1)). The results revealed a high  
74 degree of direction selectivity of  $\approx 0.8$  for GCaMP6f at slower velocities, compared to a direction  
75 selectivity of  $\approx 0.4$  for Arclight (figure 1E). For both GCaMP6f and Arclight signals, direction selectivity  
76 decreased with increasing velocity.

77 Next, instead of gratings, we used moving bright edges with all other stimulus parameters  
78 remaining the same (figure 1C). As the edge moves upward on the screen, it crosses the receptive  
79 field of T4c neurons ( $\approx 15^{\circ}$ ) only once. Hence, there was only a single peak in the response. The  
80 peak response decreased with increasing stimulus speed for GCaMP6f, while the peak response  
81 remained almost constant for Arclight throughout all speeds (figure 1D). When comparing edge  
82 responses moving along preferred and null directions, GCaMP6f showed negligible responses in  
83 null direction while Arclight revealed considerable responses to null direction stimuli. The direction  
84 selectivity index was again much higher for GCaMP6f compared to Arclight (figure 1F). Together  
85 these results show that GCaMP6f signals have a high level of direction selectivity compared to  
86 Arclight signals, both for grating and edge stimuli.

87 The stimulus strength was further varied by changing the contrast between bright and dark  
88 bars for gratings and between moving edge and background for edge stimuli. We measured  
89 Arclight and GCaMP6f responses to gratings moving at  $30^{\circ}s^{-1}$  at four different contrasts (figure 2A).  
90 Increasing contrast resulted in an increase in response for both Arclight and GCaMP6f. GCaMP6f

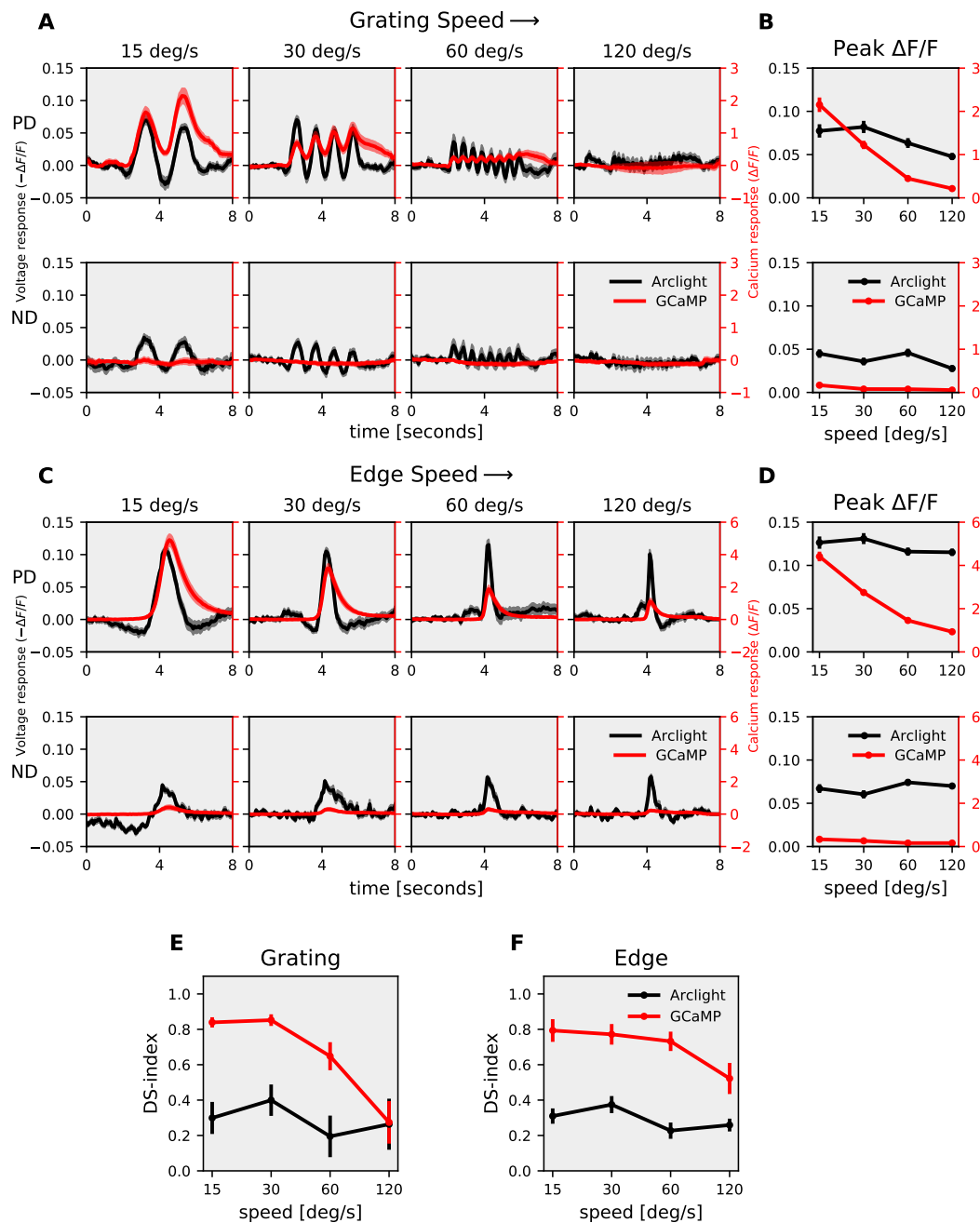


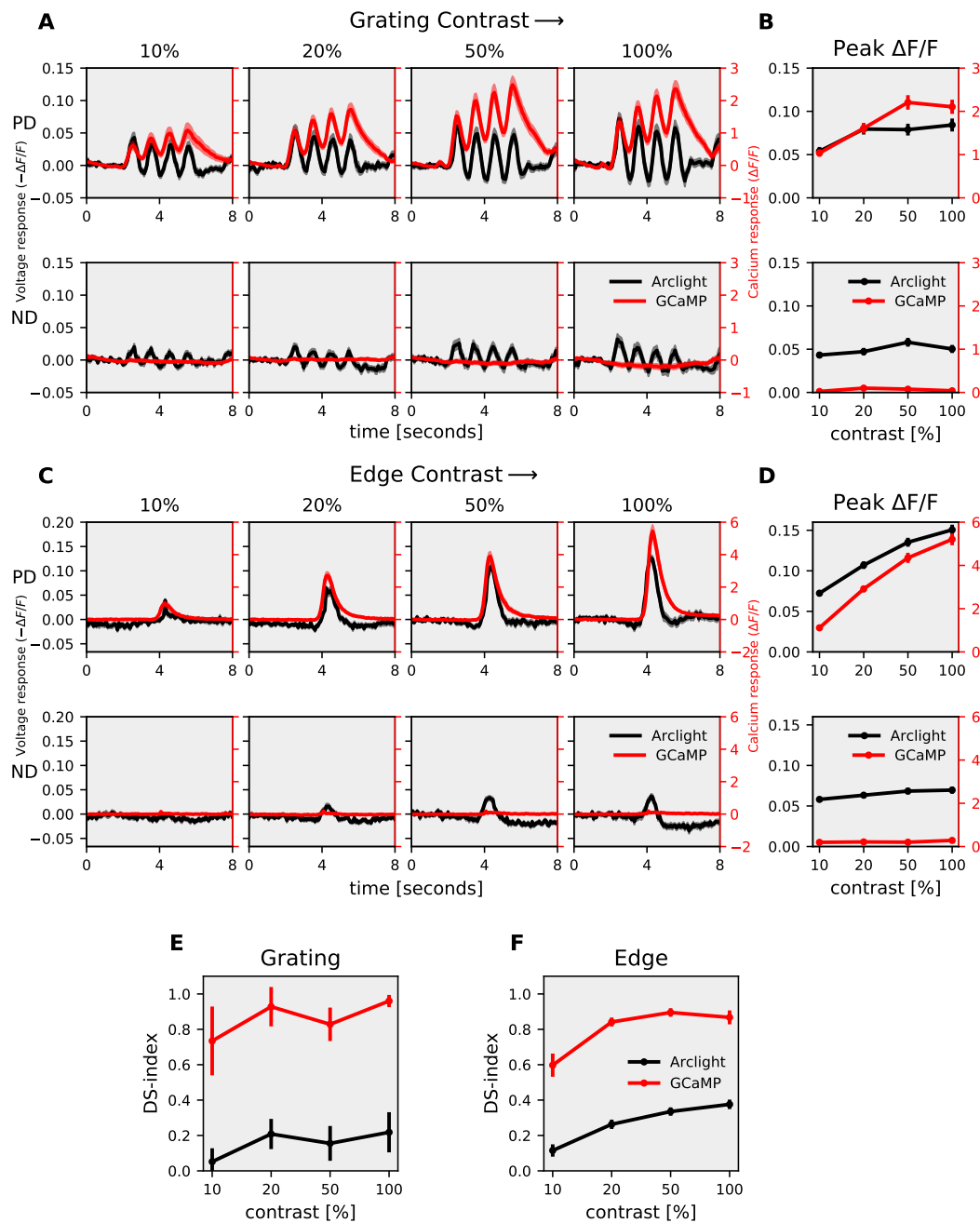
**Figure 1. T4c speed dependence :** (A) T4c Arclight (black) and GCaMP6f (red) responses to grating moving in PD (top row) and ND (bottom row) at 4 different speeds. The plots have twin y-axis. The left y-axis of the plot represents voltage responses i.e. changes in Arclight fluorescence ( $-\Delta F/F$ ) and the right y-axis of the plot represents calcium responses i.e. changes in GCaMP6f fluorescence ( $\Delta F/F$ ) (B) T4c peak responses to grating moving in PD (top) and ND (bottom) at 4 different speeds. (n = 20 ROIs from N = 10 flies for Arclight, n = 18, N = 9 for GCaMP6f) (C) T4c Arclight (black) and GCaMP6f (red) responses to ON-edge moving in PD (top row) and ND (bottom row) at 4 different speeds. (D) T4c peak responses to ON-edge moving in PD and ND at 4 different speeds. (n = 29, N = 10 for Arclight, n = 17, N = 4 for GCaMP6f) (E) Direction selectivity index (DSI) calculated as difference of peak responses in PD and ND divided by the sum of peak responses for grating. (F) Direction selectivity index (DSI) for ON-edge. All data shows the mean  $\pm$  SEM. PD: preferred direction, ND: null direction.

signals were modulated at the temporal frequency of the grating but showed an additional rise over time. This slow increase was not observed in Arclight signals. We also measured Arclight and GCaMP6f responses to ON edges moving at the same speed of  $30^{\circ}\text{s}^{-1}$  but having different contrasts (figure 2C). The peak response (maximum  $\Delta F/F$ ) increased with increasing contrast (figure 2D). Similar to previous experiments, the direction selectivity index was much higher for GCaMP6f ( $\approx 0.9$ ) compared to that for Arclight ( $\approx 0.4$ ) (figure 2E,F).

In the results presented so far we compared responses for two directions only, i.e. along the preferred (upward) and along the null direction (downward). We next extended the comparison to motion along 12 directions, from  $0^{\circ}$  to  $360^{\circ}$  in steps of  $30^{\circ}$ . For this comparison, we determined the normalized peak responses of Arclight and GCaMP6f signals to gratings moving in 12 directions at 4 different speeds and 4 different contrasts, respectively (figure 3A, B). The directional tuning was much sharper for GCaMP6f compared to Arclight. To quantify this we calculated the directional tuning index  $L_{dir}$  (Mazurek *et al.* 2014) for each speed and each contrast as the vector sum of the peak responses divided by the sum of all individual vector magnitudes (Materials and Methods equation (2)). In general, the directional tuning indices again were much higher for GCaMP6f ( $\approx 0.6$ ) compared to that of Arclight ( $\approx 0.2$ ) (figure 3C, D). Together these results show that GCaMP6f signals have a higher degree of directional tuning across different speeds and contrasts than Arclight.

How does the voltage to calcium transformation lead to calcium signals with significantly higher directional tuning compared to voltage signals? To address this question, we constructed an algorithmic model (figure 4) which takes Arclight signals as inputs and outputs GCaMP signal. In order to find the optimal parameter values, we first defined an error function. For each stimulus condition, the error was calculated as the sum of the squared difference between the model and experimental data at each time-point (Materials and Methods equation (3)). There were a total of 112 stimulus conditions: gratings speed (48), gratings contrast (48), edge speed (8) and edge contrast (8). The total error amounted to the sum of errors across all stimulus conditions (Materials and Methods equation (4)). We defined the model error as the total error divided by the power of the data (Materials and Methods equation (5)). We then found the optimal parameters values of the model that correspond to the minimum total error using Python SciPy optimize minimize function (Virtanen *et al.* 2020).

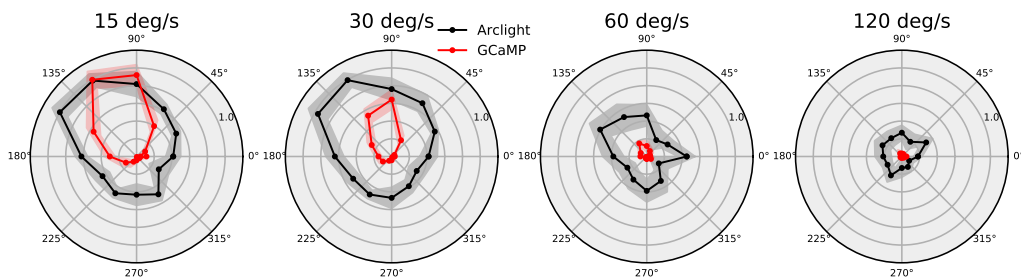
We started with a simple model (figure 4A). The model first passes the Arclight signal through a high-pass filter. The high-pass filter brings the input Arclight signal closer to the actual voltage signal by removing the slowly fluctuating Arclight indicator dynamics. This is followed by a threshold, assuming that the voltage changes below a certain threshold does not affect the calcium level in the cell. Now, few experimental observations which we took into consideration for building up the model further were as follows : First, the GCaMP6f response to gratings showed modulations only for slower speeds, whereas Arclight response had modulations even at faster speeds (figure 1A). This suggests that the GCaMP6f signal is a low-pass filtered version of the Arclight signal. In the simple model, we used a single low-pass filter followed by a gain and time-shift. Multiplication with a gain factor was required since GCaMP6f signals have a much higher magnitude compared to Arclight. Arclight and GCaMP6f responses were recorded from cells in different flies with different receptive fields, therefore the responses had different phases, and a time-shift was necessary to align the signals. However, the simple model with single low-pass filter could not reproduce responses across all stimuli. The model error for the complete dataset fit for the simple model was around 34%. Specifically, the simple model failed to suppress the ND-responses and to reproduce the edge responses. The directional tuning index  $L_{dir}$  was much smaller for the simple model compared to the experimental data (figure 5E,F). Second, the GCaMP6f responses in addition to modulation also had a steady rise over time whereas Arclight signal only had modulations (figure 1A, 2A). For reproducing the edge responses and modulation in grating responses, the model needed a low-pass filter with a small time constant. However to simulate the steady rise in the grating signal, a low-pass filter with a large time constant was necessary. Hence, we combined the output of two low-pass filters. Summing up the low-pass filter outputs did not lead to much improvement.



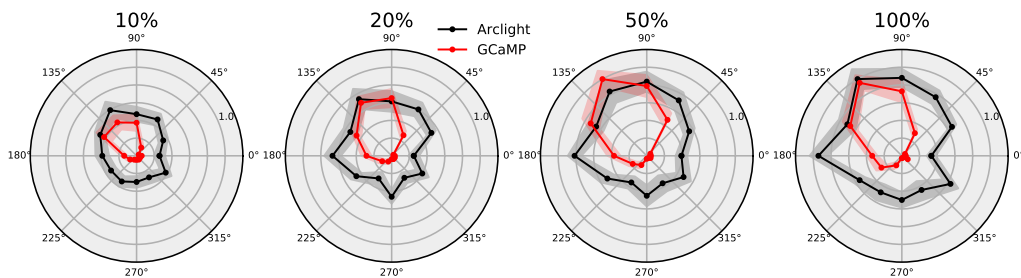
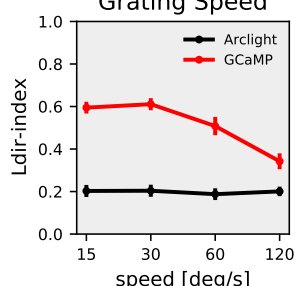
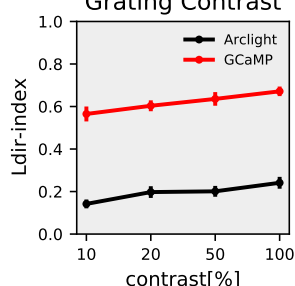
**Figure 2. T4c contrast dependence :** (A) T4c Arclight (black) and GCaMP6f (red) responses to grating moving in PD (top row) and ND (bottom row) at 4 different contrasts. The left y-axis of the plot represents voltage responses i.e. changes in Arclight fluorescence ( $-\Delta F/F$ ) and the right y-axis of the plot represents calcium responses i.e. changes in GCaMP6f fluorescence ( $\Delta F/F$ ) (B) T4c peak responses to grating moving in PD (top) and ND (bottom) at 4 different contrasts. (n = 23 ROIs from N = 11 flies for Arclight, n = 22, N = 9 for GCaMP6f) (C) T4c Arclight (black) and GCaMP6f (red) responses to ON-edge moving in PD (top row) and ND (bottom row) at 4 different contrasts. (D) T4c peak responses to ON-edge moving in PD and ND at 4 different contrasts. (n = 36, N = 5 for Arclight, n = 41, N = 7 for GCaMP6f) (E) Direction selectivity index (DSI) calculated as difference of peak responses in PD and ND divided by the sum of peak responses for grating. (F) Direction Selectivity Index (DSI) for ON-edge. All data shows the mean  $\pm$  SEM.

**A**

Grating Speed →

**B**

Grating Contrast →

**C Grating Speed****D Grating Contrast**

**Figure 3. T4c direction tuning :** (A) T4c Arclight (black) and GCaMP6f (red) normalized peak responses to grating moving in 12 directions at 4 different speeds. ( $n = 20$  ROIs from  $N = 10$  flies for Arclight,  $n = 18$ ,  $N = 9$  for GCaMP6f) (B) T4c Arclight (black) and GCaMP6f (red) normalized peak responses to grating moving in 12 directions at 4 different contrasts. ( $n = 23$ ,  $N = 11$  for Arclight,  $n = 22$ ,  $N = 9$  for GCaMP6f) (C) The directional tuning index  $L_{dir}$  for grating moving at 4 different speeds. The directional tuning index is calculated as the vector sum of the peak responses divided by the sum of all individual vector magnitudes. (D) The directional tuning index for grating at 4 different contrasts. All data shows the mean  $\pm$  SEM measured in 5 different flies.

## A Simple Model



## B Multiplicative Model

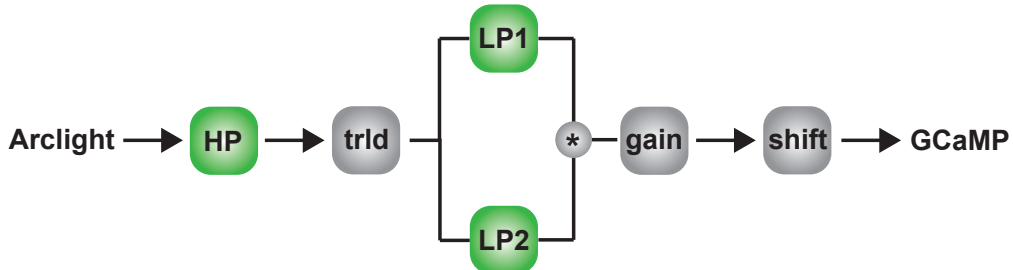


**Figure 4. Models for voltage to calcium transformation :** (A) Simple model consisting of High-Pass filter (HP), threshold (trld), Low-Pass filter (LP), gain and shift. (B) Multiplicative model combining output of two low-pass filters via multiplication.

142 However, combining both outputs from the low-pass filters with a multiplication led to significant  
 143 decrease in the error. The model error for the multiplicative model (figure 4B) then was only at  
 144 around 20%.

145 The multiplicative model thus has in total 6 parameters - high-pass filter time constant, threshold,  
 146 low-pass filter 1 time constant, low-pass filter 2 time constant, gain and shift. The multiplicative  
 147 model was able to reproduce calcium signals across different visual stimuli (figure 5). It could  
 148 reproduce both the modulation as well as slow rise in the GCaMP6f signal in response to gratings  
 149 (figure 5A). The multiplicative model could also reproduce the ON edge speed tuning responses  
 150 across different speeds (figure 5C,D). The directional tuning index  $L_{dir}$  were similar for multiplicative  
 151 model and experimental data across slower speeds and all contrasts (figure 5E,F).

152 Is the slow rise in GCaMP6f signals over time due to the properties of T4 cells or due to the  
 153 properties of GCaMP6f? To answer this question we used a faster version of the calcium indicator  
 154 GCaMP8f (Zhang et al. 2020). GCaMP8f was expressed in T4c cells using the same driver line. The  
 155 experiments were repeated using grating stimuli in 12 directions at 4 speeds and ON edges moving  
 156 in PD and ND. T4c cells GCaMP8f responses were similar to GCaMP6f responses but faster. As  
 157 with GCaMP6f, GCaMP8f signals had modulation and slow rise over time. We further compared  
 158 the model parameters values for GCaMP6f data fit and GCaMP8f data fit (figure 6). The model  
 159 parameters were similar, but with time constants having smaller values for GCaMP8f as it is a faster  
 160 indicator. Therefore, the slow rise in the calcium signal is not due to the properties of GCaMP6f  
 161 indicator.

162 To reproduce the calcium responses for direction-selective T4c cells under all stimuli conditions,  
 163 a multiplicative model was required. For non-direction-selective cells, what does the voltage to  
 164 calcium transformation look like, and is the simple model able to replicate the calcium response  
 165 for these cells? In order to answer this question, we expressed Arclight & GCaMP6f in medulla  
 166 neurons Mi1 & Tm3 cells, which are both non-direction-selective. Mi1 and Tm3 are pre-synaptic to  
 167 T4 cells and have ON-center receptive field (Behnia et al. 2014; Arenz et al. 2017). We measured  
 168 Mi1, Tm3 Arclight (black) and GCaMP6f (red) responses to gratings moving at 4 different speeds  
 169 and to gratings moving at 4 different contrasts (figure 7). The gratings were moved in only one

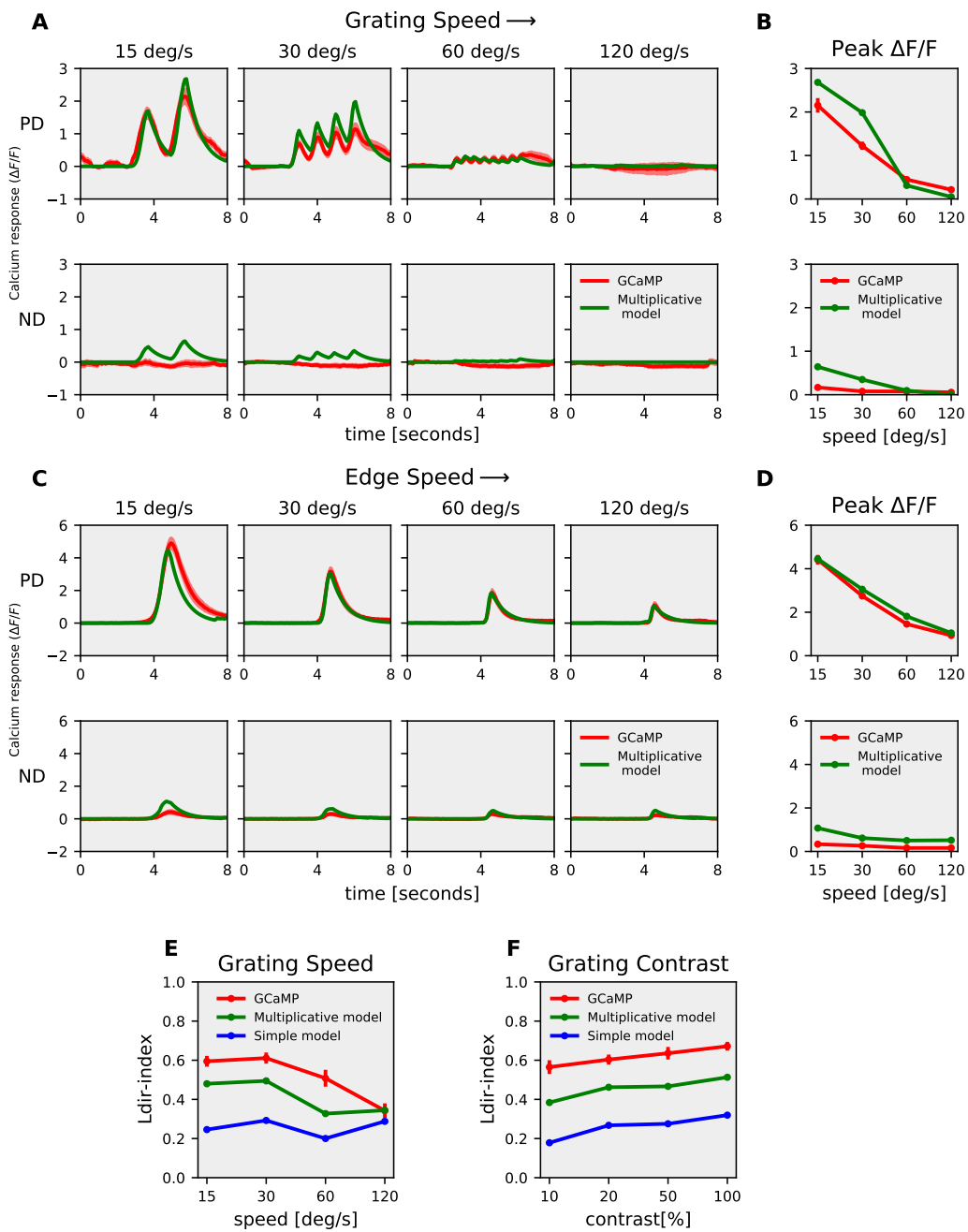


**Figure 5. Model responses :** (A) T4c GCaMP6f (red) and multiplicative model (green) responses to grating moving in PD (top row) and ND (bottom) at 4 different speeds. (B) T4c GCaMP6f and model peak responses to grating moving in PD (top) and ND(bottom) at 4 different speeds. (C) T4c GCaMP6f (red) and multiplicative model (green) responses to ON-edge moving in PD (top row) and ND (bottom row) at 4 different speeds. (D) T4c GCaMP6f and model peak responses to ON-edge moving in PD (top) and ND (bottom) at 4 different speeds. (E, F) The directional tuning index  $L_{dir}$  for GCaMP6f (red), multiplicative (green) and simple (blue) model for grating moving in 12 directions at 4 different speeds and at 4 different contrasts respectively.

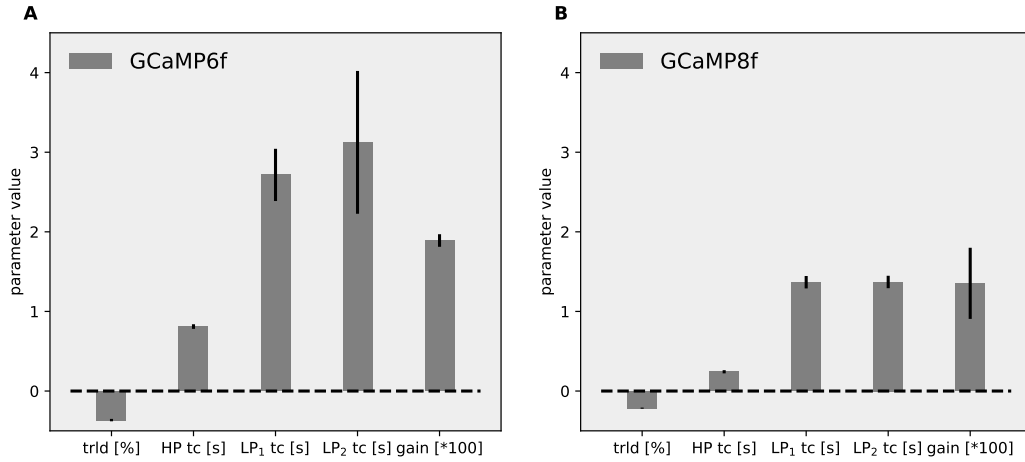


**Figure 6. Model parameters for GCaMP6f (A) and GCaMP8f (B)**: Data shows mean  $\pm$  SD for optimal parameters for the multiplicative model. The data were fit for grating moving in 12 directions and 4 speeds, and for ON-edge moving in PD and ND at 4 speeds. trld : threshold, HP : High Pass, LP : Low Pass, tc : Time constant

170 direction, since the direction does not affect non-direction-selective cells' responses. Contrary to T4,  
 171 Mi1 GCaMP6f responses had only modulation without a slow increase over time (figure 7A). Tm3  
 172 GCaMP responses did not increase over time, and showed only modulation for gratings moving at  
 173  $15^{\circ}s^{-1}$ . For gratings moving at  $30^{\circ}s^{-1}$  and  $60^{\circ}s^{-1}$ , there was an increase in Tm3 GCaMP6f response  
 174 over time, but the Arclight response also already had a slow increment over time (figure 7A). Similar  
 175 to T4, the peak response for Mi1 and Tm3 decreased with an increase in speed and increased  
 176 with an increase in contrast (figure 7B, D). Together, these results show that voltage to calcium  
 177 transformation causes GCaMP6f response increment over time only for direction-selective T4 cells  
 178 and not for non-direction-selective Mi1 and Tm3 cells.

179 Next, we used the model described in figure 4 to reproduce Mi1 and Tm3 calcium responses  
 180 using their Arclight responses. As discussed earlier, the simple model (figure 4A) with single  
 181 low-pass filter was not able to reproduce T4 calcium responses across all stimuli. However, for  
 182 Mi1 and Tm3, the simple model with a single low-pass filter was able to reproduce the calcium  
 183 responses across all stimuli conditions (figure 8). The model also accurately replicated the speed  
 184 and contrast tuning for Mi1 and Tm3 (figure 8B, D). We further compared the model error for  
 185 simple and multiplicative model for Mi1, Tm3 and T4c data (figure 9). The model error for Mi1 and  
 186 Tm3 for simple model was  $\approx 6.5\%$  and  $\approx 5.9\%$  respectively compared to  $\approx 11.9\%$  and  $\approx 7\%$  for the  
 187 multiplicative model. Thus, the simple model already performed well for Mi1 and Tm3 dataset,  
 188 and changing to multiplicative model did not improve the performance. For the T4c dataset the  
 189 model error was  $\approx 34\%$  and  $\approx 21\%$  for the simple and multiplicative model respectively. Hence, the  
 190 multiplicative model with two low-pass filters performed better for T4c dataset whereas for Mi1 and  
 191 Tm3 the Simple model with single low-pass filter was sufficient to reproduce the calcium responses.  
 192 This suggests that voltage-to-calcium transformation is more complex for direction-selective cell T4  
 193 than for the non-direction-selective cells Mi1 and Tm3.

## 194 Discussion

195 Neuronal signaling and information processing involves the transformation of membrane voltage  
 196 into calcium signals, which lead to transmitter release. Computations can occur at different stages in  
 197 the signalling cascade: 1.) dendritic integration and processing of voltage signals. 2.) transformation  
 198 from voltage to calcium and 3.) between calcium and neurotransmitter release. In this study, we

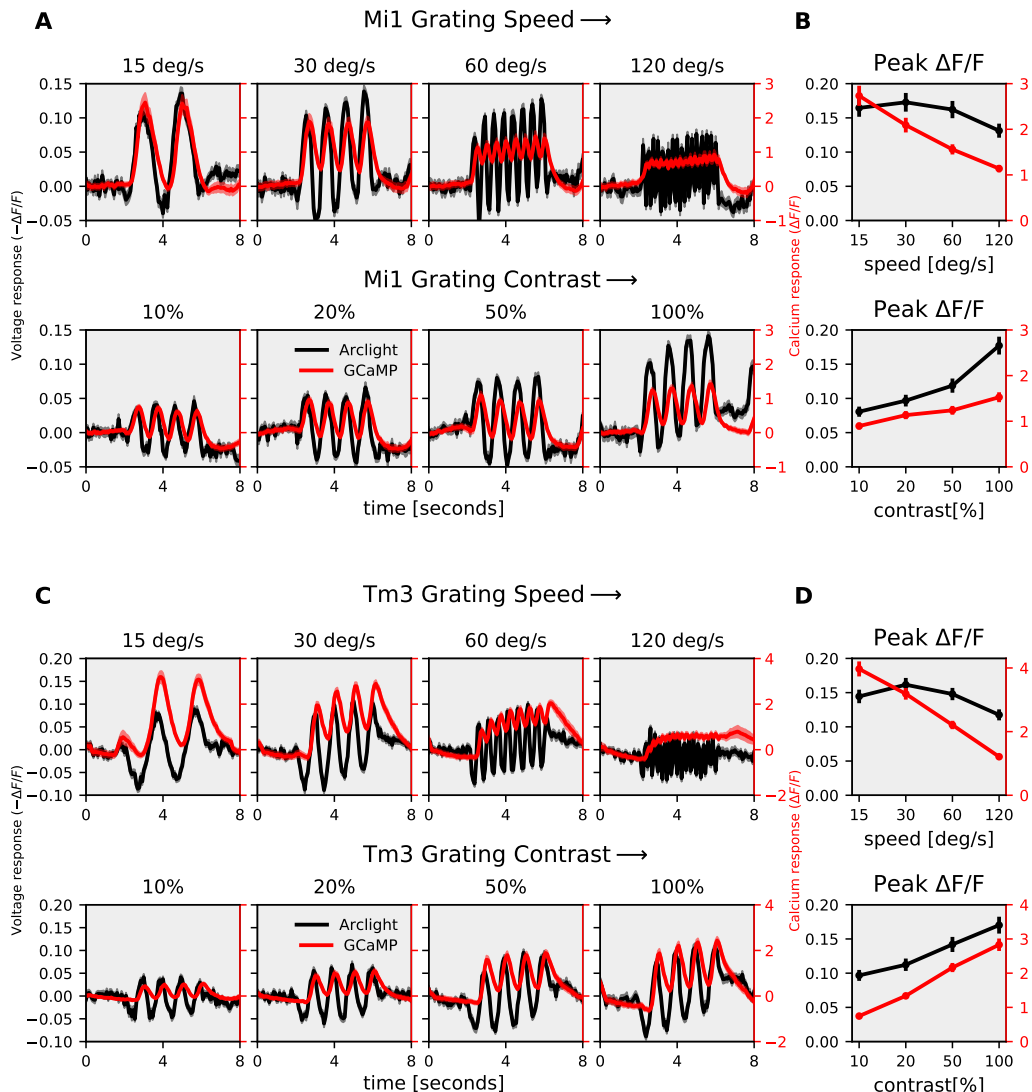


**Figure 7. Mi1, Tm3 speed and contrast dependence :** (A) Mi1 Arclight (black) and GCaMP6f (red) responses to grating moving at 4 different speeds (top row) and 4 different contrasts (bottom row). The left y-axis of the plot represents voltage responses i.e. changes in Arclight fluorescence ( $-\Delta F/F$ ) and the right y-axis of the plot represents calcium responses i.e. changes in GCaMP6f fluorescence ( $\Delta F/F$ ) (B) Mi1 peak responses to grating moving at 4 different speeds ( $n = 24$  ROIs from  $N = 5$  flies for Arclight,  $n = 19$ ,  $N = 8$  for GCaMP ) and 4 different contrasts ( $n = 24$ ,  $N = 5$  for Arclight,  $n = 22$ ,  $N = 8$  for GCaMP). (C) Tm3 Arclight (black) and GCaMP6f (red) responses to grating moving at 4 different speeds (top row) and 4 different contrasts (bottom row). (D) Tm3 peak responses to grating moving at 4 different speeds ( $n = 52$ ,  $N = 5$  for Arclight,  $n = 37$ ,  $N = 4$  for GCaMP) and 4 different contrasts ( $n = 35$ ,  $N = 5$  for Arclight,  $n = 36$ ,  $N = 4$  for GCaMP). All data shows the mean  $\pm$  SEM.

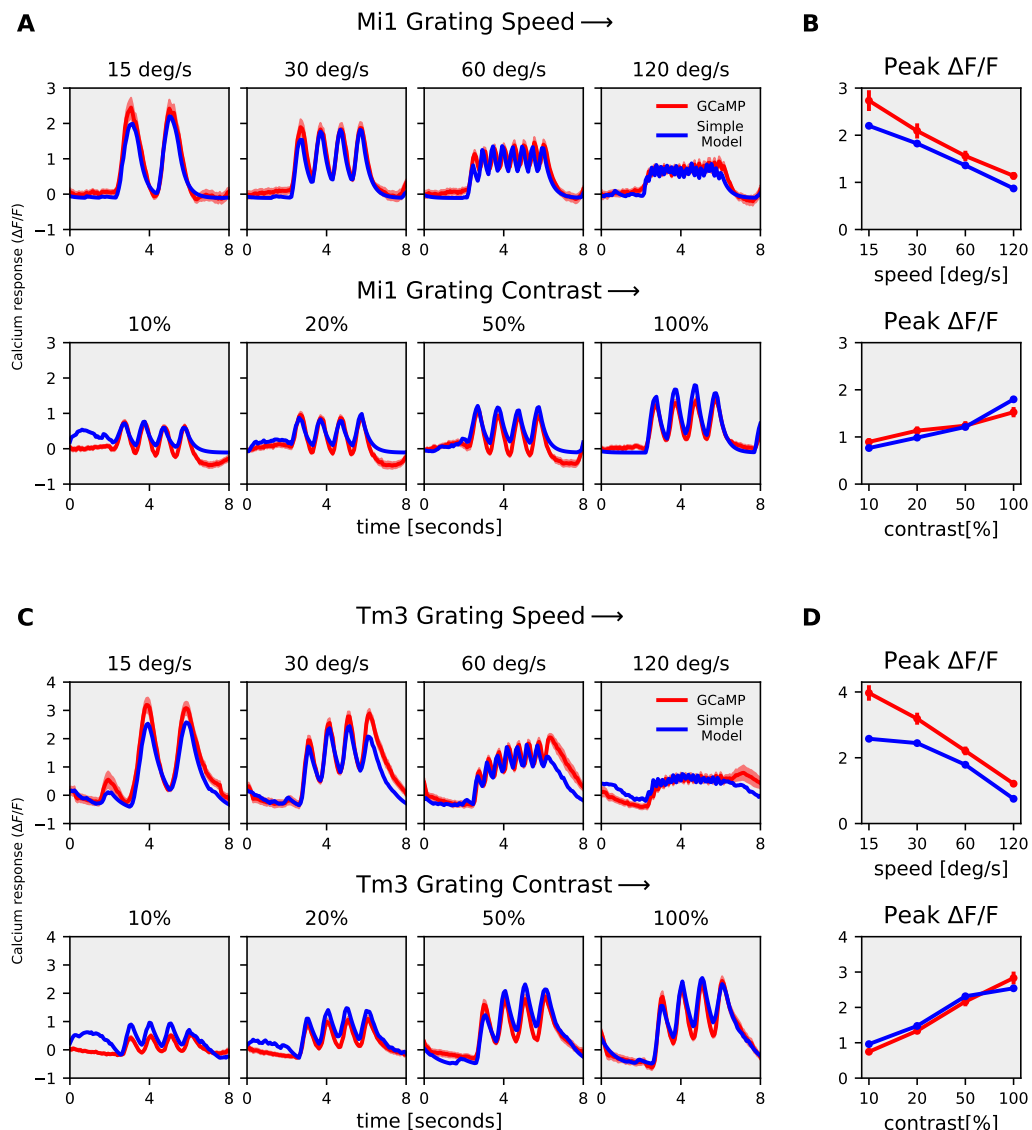


**Figure 8. Mi1, Tm3 Simple model responses :** (A) Mi1 GCaMP6f (red) and simple model (blue) responses to gratings moving at 4 different speeds (top row) and to gratings moving at 4 different contrasts (bottom row). (B) Mi1 GCaMP6f and model peak responses to gratings moving at 4 different speeds (top) and 4 different contrasts (bottom). (C) Tm3 GCaMP6f (red) and simple model (blue) responses to gratings moving at 4 different speeds (top row) and to gratings moving at 4 different contrasts (bottom row). (D) Tm3 GCaMP6f and model peak responses to gratings moving at 4 different speeds (top) and 4 different contrasts (bottom).

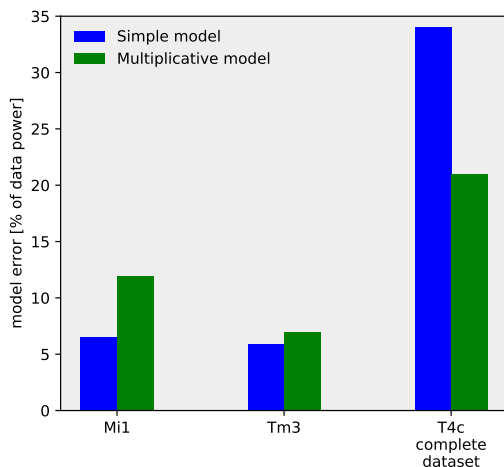


**Figure 9. Model error for the simple and multiplicative model :** The model error for the simple model (blue) and multiplicative model (green). Mi1 and Tm3 dataset consists of gratings at 4 different speeds and contrast moving in a single direction. T4c complete dataset consists of gratings moving in 12 different directions, and ON edge moving in PD, ND at 4 different speeds and contrasts i.e. a total of 112 stimuli conditions.

199 explored the transformation of voltage to calcium in T4-cells, the first direction-selective neurons in  
200 the *Drosophila* ON motion vision pathway.

201 We found that the voltage to calcium transformation in T4c neurons enhances their direction  
202 selectivity: calcium signals in T4c cells have a significantly higher direction selectivity and tuning  
203 compared to membrane voltage across different stimuli conditions (figure 1-3). The direction  
204 selectivity index for calcium signals compared with voltage signals for a few stimuli conditions was  
205 previously found to be higher in a study in T5 cells using ASAP2f as an optical voltage indicator  
206 (Wienecke *et al.* 2018). As calcium is required for neurotransmitter release, this is expected to  
207 increase the direction selectivity of T4/T5 cells' output signals. In the lobula plate, T4/T5 cells  
208 provide inputs onto large lobula plate tangential cells that are depolarized during preferred and  
209 hyperpolarized during null direction motion (Mauss *et al.* 2014). For example, vertical system  
210 (VS) cells with dendrites in layer 4 receive direct excitatory inputs from downward tuned T4d/T5d  
211 neurons causing depolarization during motion in the downward preferred direction. These VS cells  
212 also receive indirect inhibitory inputs from upward tuned T4c/T5c neurons via glutamatergic LPi3-4  
213 neurons projecting from layer 3 to layer 4 causing hyperpolarization in VS cells during motion in the  
214 upward null direction. Upon silencing LPi3-4 neurons' synaptic output via tetanus toxin, VS neurons  
215 depolarization response in the preferred direction did not change, but the null direction response  
216 was absent (Mauss *et al.* 2015). This suggests T4/T5 do not release any transmitter in response  
217 to null direction motion, which matches our findings for the calcium responses. Thus, voltage to  
218 calcium transformation increases direction selectivity in T4/T5 cells and this enhances direction  
219 selectivity in downstream neurons.

220 Electrophysiology has been the most frequently used method to measure the membrane  
221 potential changes in neurons. However, due to the small size of neurons in the optic lobe, single-cell  
222 electrophysiological recordings of these neurons have been difficult. Genetically encoded voltage  
223 indicators (GEVIs) have evolved as powerful tools for recording changes in neuronal membrane  
224 potentials (Yang *et al.* 2016). Optical methods of monitoring brain activity are appealing because  
225 they allow simultaneous, noninvasive monitoring of activity in many individual neurons. We used  
226 a fluorescence protein (FP) voltage sensor called Arclight (Jin *et al.* 2012). Arclight is based on the  
227 fusion of the voltage-sensing domain of *Ciona intestinalis* voltage-sensitive phosphatase (Murata  
228 *et al.* 2005) and the fluorescent protein super eYFP with an A227D mutation. Arclight

229 has been shown to robustly report both subthreshold events and action potentials in genetically  
230 targeted neurons in the intact *Drosophila* brain (Cao *et al.* 2013).

231 We built a model to capture voltage to calcium transformation in T4c, Mi1, and Tm3 cells. A  
232 simple model with a single low-pass filter was able to reproduce calcium responses in non-direction-  
233 selective Mi1 and Tm3 cells (figure 8), whereas a more complex model combining the output of two  
234 low-pass filters via a multiplication was required to reproduce T4c calcium responses (figure 5). The  
235 direction selectivity for the simple model signals for T4c was lower compared to the multiplicative  
236 model. This suggests that voltage-calcium transformation in Mi1 and Tm3 cells is different from  
237 those in T4c cells.

238 The time constants for the two low-pass filters were identical for the multiplicative model for  
239 T4c data fit. Thus, these two low-pass filters in the multiplicative model could also be replaced by a  
240 single low-pass filter followed by a quadratic non-linearity. An exponent of close to 2 (exact value:  
241 2.2) was found in the parameter search for a model with a single low-pass filter followed by an  
242 exponential nonlinearity.

243 Differential expression of voltage-gated calcium channels in these cells could explain the dif-  
244 ferent voltage to calcium transformation. Voltage-gated calcium channels mediate depolarization-  
245 induced calcium influx that drives the release of neurotransmitters. The  $\alpha$ 1-subunit of the voltage-  
246 gated calcium channels forms the ion-conducting pore, which makes it distinct from other calcium  
247 channels. Three families of genes encode  $\alpha$ 1 subunits. *Drosophila* genome has one  $\alpha$ 1 subunit  
248 gene in each family:  $\alpha$ 1D ( $Ca_v$ 1), cac ( $Ca_v$ 2), and  $\alpha$ 1T ( $Ca_v$ 3) (Littleton & Ganetzky 2000; King 2007).  
249 In *Drosophila* antennal lobe projection neurons, cac ( $Ca_v$ 2) type and  $\alpha$ 1T ( $Ca_v$ 3) type voltage-gated  
250 calcium channels are involved in sustained and transient calcium currents, respectively (Gu *et al.*  
251 2009; Iniguez *et al.* 2013). According to a RNA-sequencing study (Davis *et al.* 2020),  $\alpha$ 1T ( $Ca_v$ 3)  
252 mRNA have higher expression in Mi1 (2050.16 Transcripts per Million (TPM)) compared to T4 (686.68  
253 TPM) and Tm3 (336.45 TPM). While cac ( $Ca_v$ 2) mRNA have higher expression in T4 (1298.53 TPM)  
254 compared to Mi1 (986.25 TPM) and Tm3 (817.61 TPM). Different expression of voltage-gated calcium  
255 channels could cause different voltage to calcium transformations in non-direction selective and  
256 direction-selective cells. In addition to dendritic integration of postsynaptic voltages, the specific  
257 voltage-to-calcium transformation described in this study provides an important processing step  
258 that enhances direction selectivity in the output signal of motion-sensing neurons of the fly.

## 259 Materials and Methods

### 260 Flies

261 Flies (*Drosophila melanogaster*) were raised at 25°C and 60% humidity on a 12 hour light/12 hour dark  
262 cycle on standard cornmeal agar medium. For calcium imaging experiments, genetically-encoded  
263 calcium indicator GCaMP6f (Chen *et al.* 2013) was expressed in T4 neurons with axon terminals  
264 predominantly in layer 3 of the lobula plate. Similarly for voltage imaging experiments, genetically-  
265 encoded voltage indicator Arclight (Jin *et al.* 2012) was expressed in T4 layer 3 neurons. The flies  
266 genotype were as follows :

- 267 1. T4c>GCaMP6f : w+ ; VT15785-Gal4AD / UAS-GCaMP6f; VT50384-Gal4DBD / UAS-GCaMP6f
- 268 2. T4c>Arclight : w+ ; VT15785-Gal4AD / UAS-Arclight; VT50384-Gal4DBD / +

269 For Mi1 and Tm3 experiments, the flies genotype were as follows :

- 270 1. Mi1>GCaMP6f : w+ ; R19F01-Gal4AD / UAS-GCaMP6f; R71D01-Gal4DBD / UAS-GCaMP6f
- 271 2. Mi1>Arclight : w+ ; R19F01-Gal4AD / UAS-Arclight; R71D01-Gal4DBD / +
- 272 3. Tm3>GCaMP6f : w+ ; R13E12-Gal4AD / UAS-GCaMP6f; R59C10-Gal4DBD / UAS-GCaMP6f
- 273 4. Tm3>Arclight : w+ ; R13E12-Gal4AD / UAS-Arclight; R59C10-Gal4DBD / +

### 274 Calcium & voltage imaging

275 For imaging experiments, fly surgeries were performed as previously described (Maisak *et al.* 2013).  
276 Briefly, flies were anaesthetized with CO<sub>2</sub> or on ice, fixed with their backs, legs and wings to a

277 Plexiglas holder with back of the head exposed to a recording chamber filled with fly external  
278 solution. The cuticula at the back of the head on one side of the brain was cut away with a fine  
279 hypodermic needle and removed together with air sacks covering the underlying optic lobe. The  
280 neuronal activity was then measured from the optic lobe with a custom-built 2-photon microscope  
281 as previously described (Maisak *et al.* 2013). Images were acquired at 64 x 64 pixels resolution and  
282 frame rate 13 Hz with the Scanimate software in Matlab (Pologruto *et al.* 2003).

283 **Visual stimulation**

284 For the study of visual responses of T4c cells, visual stimuli were presented on a custom-built  
285 projector-based arena as described in (Arenz *et al.* 2017). In brief : Two micro-projectors (TI DLP  
286 Lightcrafter 3000) were used to project stimuli onto the back of an opaque cylindrical screen  
287 covering 180° in azimuth and 105° in elevation of the fly's visual field. To increase the refresh rate  
288 from 60 Hz to 180 Hz (at 8 bit color depth), projectors were programmed to use only green LED  
289 (OSRAM L CG H9RN) which emits light between 500 nm to 600 nm wavelength. Two long-pass filters  
290 (Thorlabs FEL0550 and FGL550) were placed in front of each projector to restrict the stimulus light  
291 to wavelengths above 550 nm. This prevents overlap between fluorescence signal and arena light  
292 spectra. To allow only fluorescence emission spectrum to be detected, a band-pass filter (Brightline  
293 520/35) was placed in-front of the photomultiplier. Stimuli were rendered using custom written  
294 software in Python 2.7.

295 **Stimuli**

296 Stimuli were presented with 3-5 repetitions per experiment in a randomized fashion. To measure  
297 the directional and speed tuning, square-wave gratings with a spatial wavelength of 30° spanning  
298 the full extent of the stimulus arena were used. The gratings were moved in 12 different directions  
299 from 0° – 360° at 4 different speeds (15°s<sup>-1</sup>, 30°s<sup>-1</sup>, 60°s<sup>-1</sup>, 120°s<sup>-1</sup>). Similarly, to measure direction  
300 and contrast tuning, square-wave gratings with a spatial wavelength of 30° spanning the full extent  
301 of the stimulus arena were used. The gratings moved at a speed of 30°s<sup>-1</sup> in 12 different directions  
302 at 4 different contrasts (10%, 20%, 50%, 100%). Edge responses were measured using ON edge i.e.  
303 bright edge moving on a dark background with full contrast. The ON edge moved in preferred  
304 direction (upward) or null direction (downward) at 4 different speeds (15°s<sup>-1</sup>, 30°s<sup>-1</sup>, 60°s<sup>-1</sup>, 120°s<sup>-1</sup>).

305 **Data analysis**

306 Data analysis was performed using custom-written routines in Matlab and Python 2.7, 3.7. Images  
307 were automatically registered using horizontal and vertical translations to correct for the movement  
308 of brain. Fluorescence changes ( $\Delta F/F$ ) were then calculated using a standard baseline algorithm  
309 (Jia *et al.* 2011). Regions of interest (ROIs) were drawn on the average raw image manually by hand  
310 in the medulla layer M10 for signals from T4 dendrites. Averaging the fluorescence change over this  
311 ROI in space resulted in a ( $\Delta F/F$ ) time course. Voltage imaging with Arclight and calcium imaging  
312 with GCaMP6f and GCaMP8f were performed and analysed using same settings.

313 The direction selectivity was evaluated using a direction selectivity index (DSI) calculated as the  
314 difference of the peak responses to preferred and null direction, divided by the sum of the peak  
315 responses:

$$DSI = \frac{PD_{peak} - ND_{peak}}{PD_{peak} + ND_{peak}} \quad (1)$$

316 In the above measurement, only the difference in response between the two opposing directions of  
317 motion is quantified. To take into account all 12 directions of motion, we calculated the directional  
318 tuning index:

$$L_{dir} = \left| \frac{\sum_{\varphi} \vec{v}(\varphi)}{\sum_{\varphi} |\vec{v}(\varphi)|} \right| \quad (2)$$

319 where  $\vec{v}(\varphi)$  is a vector proportionally scaled with the mean response and points in the direction  
320 corresponding to the direction of motion given by the rotation angle  $\varphi$  of the stimulus (Mazurek

321 *et al.* 2014).

### 322 Model simulations

323 Custom-written Python3.7 scripts were used to simulate the models (figure 4). To calculate the  
324 optimal parameter values, we first defined an error function. For each stimulus condition ( $s_i$ ), the  
325 error was calculated as:

$$326 \quad error(s_i) = \sum_{t=0}^{t=N} (model(s_i, t) - data(s_i, t))^2 \quad (3)$$

326 The model took as input Arclight data across all 112 different stimuli conditions. Next, we summed  
327 the error for all stimuli conditions:

$$328 \quad total\ error = \sum_{i=1}^{i=112} error(s_i) \quad (4)$$

328 The model parameters were initialized with random values within the defined parameter bounds.  
329 Python SciPy optimize minimize function then used the L-BFGS-B (Limited Broyden Fletcher Goldfarb  
330 Shanno) algorithm to find the parameter values corresponding to the minimum total error. A total  
331 of 300 runs were performed, and the parameter values that corresponded to the run with the  
332 lowest error were used to produce the final output signals. To compare the model performances,  
333 we calculated the model error as:

$$334 \quad model\ error [\% of data power] = \frac{total\ error}{\sum_{i=1}^{i=112} (data(s_i))^2} * 100 \quad (5)$$

### 334 References

- 335 1. Denk, W., Strickler, J. H. & Webb, W. W. Two-photon laser scanning fluorescence microscopy. *Science* **248**, 73–76 (1990). doi: [10.1126/science.2321027](https://doi.org/10.1126/science.2321027)
- 336 2. Littleton, J. T. & Ganetzky, B. Ion channels and synaptic organization: analysis of the Drosophila genome. *Neuron* **26**, 35–43 (2000). doi: [10.1016/s0896-6273\(00\)81135-6](https://doi.org/10.1016/s0896-6273(00)81135-6)
- 337 3. Chapman, E. R. Synaptotagmin: a Ca<sup>2+</sup> sensor that triggers exocytosis? *Nature Reviews Molecular Cell Biology* **3**, 498–508 (2002). doi: [10.1038/nrm855](https://doi.org/10.1038/nrm855)
- 338 4. Pologruto, T. A., Sabatini, B. L. & Svoboda, K. ScanImage: flexible software for operating laser scanning microscopes. *Biomedical engineering online* **2**, 1–9 (2003). doi: [10.1186/1475-925X-2-13](https://doi.org/10.1186/1475-925X-2-13)
- 339 5. Murata, Y., Iwasaki, H., Sasaki, M., Inaba, K. & Okamura, Y. Phosphoinositide phosphatase activity coupled to an intrinsic voltage sensor. *Nature* **435**, 1239–1243 (2005). doi: [10.1038/nature03650](https://doi.org/10.1038/nature03650)
- 340 6. King, G. F. Modulation of insect CaV channels by peptidic spider toxins. *Toxicon* **49**, 513–530 (2007). doi: [10.1016/j.toxicon.2006.11.012](https://doi.org/10.1016/j.toxicon.2006.11.012)
- 341 7. Di Maio, V. Regulation of information passing by synaptic transmission: a short review. *Brain research* **1225**, 26–38 (2008). doi: [10.1016/j.brainres.2008.06.016](https://doi.org/10.1016/j.brainres.2008.06.016)
- 342 8. Gu, H. *et al.* Cav2-type calcium channels encoded by cac regulate AP-independent neurotransmitter release at cholinergic synapses in adult Drosophila brain. *Journal of neurophysiology* **101**, 42–53 (2009). doi: [10.1152/jn.91103.2008](https://doi.org/10.1152/jn.91103.2008)
- 343 9. Joesch, M., Schnell, B., Raghu, S. V., Reiff, D. F. & Borst, A. ON and OFF pathways in Drosophila motion vision. *Nature* **468**, 300–304 (2010). doi: [10.1038/nature09545](https://doi.org/10.1038/nature09545)
- 344 10. Eichner, H., Joesch, M., Schnell, B., Reiff, D. F. & Borst, A. Internal structure of the fly elementary motion detector. *Neuron* **70**, 1155–1164 (2011). doi: [10.1016/j.neuron.2011.03.028](https://doi.org/10.1016/j.neuron.2011.03.028)
- 345 11. Jia, H., Rochefort, N. L., Chen, X. & Konnerth, A. In vivo two-photon imaging of sensory-evoked dendritic calcium signals in cortical neurons. *Nature protocols* **6**, 28–35 (2011). doi: [10.1038/nprot.2010.169](https://doi.org/10.1038/nprot.2010.169)

- 360 12. Jin, L. *et al.* Single action potentials and subthreshold electrical events imaged in neurons with a  
361 fluorescent protein voltage probe. *Neuron* **75**, 779–785 (2012). doi: [10.1016/j.neuron.2012.06.040](https://doi.org/10.1016/j.neuron.2012.06.040)
- 362 13. Cao, G. *et al.* Genetically targeted optical electrophysiology in intact neural circuits. *Cell* **154**,  
363 904–913 (2013). doi: [10.1016/j.cell.2013.07.027](https://doi.org/10.1016/j.cell.2013.07.027)
- 364 14. Chen, T.-W. *et al.* Ultrasensitive fluorescent proteins for imaging neuronal activity. *Nature* **499**,  
365 295–300 (2013). doi: [10.1038/nature12354](https://doi.org/10.1038/nature12354)
- 366 15. Iniguez, J., Schutte, S. S. & O'Dowd, D. K. Cav3-type  $\alpha$ 1T calcium channels mediate transient  
367 calcium currents that regulate repetitive firing in Drosophila antennal lobe PNs. *Journal of*  
368 *neurophysiology* **110**, 1490–1496 (2013). doi: [10.1152/jn.00368.2013](https://doi.org/10.1152/jn.00368.2013)
- 369 16. Maisak, M. S. *et al.* A directional tuning map of Drosophila elementary motion detectors. *Nature*  
370 **500**, 212–216 (2013). doi: [10.1038/nature12320](https://doi.org/10.1038/nature12320)
- 371 17. Behnia, R., Clark, D. A., Carter, A. G., Clandinin, T. R. & Desplan, C. Processing properties of  
372 ON and OFF pathways for Drosophila motion detection. *Nature* **512**, 427–430 (2014). doi:  
373 [10.1038/nature13427](https://doi.org/10.1038/nature13427)
- 374 18. Mauss, A. S., Meier, M., Serbe, E. & Borst, A. Optogenetic and pharmacologic dissection of  
375 feedforward inhibition in Drosophila motion vision. *Journal of Neuroscience* **34**, 2254–2263  
376 (2014). doi: [10.1523/JNEUROSCI.3938-13.2014](https://doi.org/10.1523/JNEUROSCI.3938-13.2014)
- 377 19. Mazurek, M., Kager, M. & Van Hooser, S. D. Robust quantification of orientation selectivity and  
378 direction selectivity. *Frontiers in neural circuits* **8**, 92 (2014). doi: [10.3389/fncir.2014.00092](https://doi.org/10.3389/fncir.2014.00092)
- 379 20. Mauss, A. S. *et al.* Neural circuit to integrate opposing motions in the visual field. *Cell* **162**,  
380 351–362 (2015). doi: [10.1016/j.cell.2015.06.035](https://doi.org/10.1016/j.cell.2015.06.035)
- 381 21. Yang, H. H. *et al.* Subcellular imaging of voltage and calcium signals reveals neural processing  
382 in vivo. *Cell* **166**, 245–257 (2016). doi: [10.1016/j.cell.2016.05.031](https://doi.org/10.1016/j.cell.2016.05.031)
- 383 22. Arenz, A., Drews, M. S., Richter, F. G., Ammer, G. & Borst, A. The temporal tuning of the  
384 Drosophila motion detectors is determined by the dynamics of their input elements. *Current*  
385 *Biology* **27**, 929–944 (2017). doi: [10.1016/j.cub.2017.01.051](https://doi.org/10.1016/j.cub.2017.01.051)
- 386 23. Wienecke, C. F., Leong, J. C. & Clandinin, T. R. Linear summation underlies direction selectivity  
387 in Drosophila. *Neuron* **99**, 680–688 (2018). doi: [10.1016/j.neuron.2018.07.005](https://doi.org/10.1016/j.neuron.2018.07.005)
- 388 24. Borst, A., Haag, J. & Mauss, A. S. How fly neurons compute the direction of visual motion.  
389 *Journal of Comparative Physiology A* **206**, 109–124 (2020). doi: [10.1007/s00359-019-01375-9](https://doi.org/10.1007/s00359-019-01375-9)
- 390 25. Davis, F. P. *et al.* A genetic, genomic, and computational resource for exploring neural circuit  
391 function. *eLife* **9**, e50901 (2020). doi: [10.7554/eLife.50901](https://doi.org/10.7554/eLife.50901)
- 392 26. Luo, L. *Principles of Neurobiology* (Garland Science, 2020). doi: [10.1201/9781003053972](https://doi.org/10.1201/9781003053972)
- 393 27. Virtanen, P. *et al.* SciPy 1.0: fundamental algorithms for scientific computing in Python. *Nature*  
394 *methods* **17**, 261–272 (2020). doi: [10.1038/s41592-019-0686-2](https://doi.org/10.1038/s41592-019-0686-2)
- 395 28. Zhang, Y. *et al.* jGCaMP8 Fast genetically encoded calcium indicators. *Online resource* (2020).  
396 doi: [10.25378/janelia.13148243.v4](https://doi.org/10.25378/janelia.13148243.v4)
- 397 29. Groschner, L. N., Malis, J. G., Zuidinga, B. & Borst, A. A biophysical account of multiplication by  
398 a single neuron. *Nature* **603**, 119–123 (2022). doi: [10.1038/s41586-022-04428-3](https://doi.org/10.1038/s41586-022-04428-3)

## BIBLIOGRAPHY

1. Ramón y Cajal, S. & Sánchez, D. *Contribución al conocimiento de los centros nerviosos de los insectos / por S.R. Cajal y D. Sánchez.* 1–180 (Imprenta de Hijos de Nicolás Moya, Madrid : Nov. 1915). doi: [10.5962/bhl.title.37839](https://doi.org/10.5962/bhl.title.37839)
2. Hodgkin, A. L. & Huxley, A. F. A quantitative description of membrane current and its application to conduction and excitation in nerve. *The Journal of physiology* **117**, 500 (1952). doi: [10.1113/jphysiol.1952.sp004764](https://doi.org/10.1113/jphysiol.1952.sp004764)
3. Baker, P., Hodgkin, A. & Ridgway, E. Depolarization and calcium entry in squid giant axons. *The Journal of physiology* **218**, 709–755 (1971). doi: [10.1113/jphysiol.1971.sp009641](https://doi.org/10.1113/jphysiol.1971.sp009641)
4. Rubin, G. M. & Spradling, A. C. Genetic transformation of *Drosophila* with transposable element vectors. *Science* **218**, 348–353 (1982). doi: [10.1126/science.6289436](https://doi.org/10.1126/science.6289436)
5. Buchner, E., Buchner, S. & Bülthoff, I. Deoxyglucose mapping of nervous activity induced in *Drosophila* brain by visual movement. *Journal of Comparative Physiology A* **155**, 471–483 (1984). doi: [10.1007/BF00611912](https://doi.org/10.1007/BF00611912)
6. Papazian, D. M., Schwarz, T. L., Tempel, B. L., Jan, Y. N. & Jan, L. Y. Cloning of genomic and complementary DNA from Shaker, a putative potassium channel gene from *Drosophila*. *Science* **237**, 749–753 (1987). doi: [10.1126/science.2441470](https://doi.org/10.1126/science.2441470)
7. Fischbach, K.-F. & Dittrich, A. The optic lobe of *Drosophila melanogaster*. I. A Golgi analysis of wild-type structure. *Cell and tissue research* **258**, 441–475 (1989). doi: [10.1007/BF00218858](https://doi.org/10.1007/BF00218858)
8. Covarrubias, M., Wei, A. & Salkoff, L. Shaker, Shal, Shab, and Shaw express independent K<sup>+</sup> current systems. *Neuron* **7**, 763–773 (1991). doi: [10.1016/0896-6273\(91\)90279-9](https://doi.org/10.1016/0896-6273(91)90279-9)
9. Brand, A. H. & Perrimon, N. Targeted gene expression as a means of altering cell fates and generating dominant phenotypes. *Development* **118**, 401–415 (1993). doi: [10.1242/dev.118.2.401](https://doi.org/10.1242/dev.118.2.401)
10. Egelhaaf, M. & Borst, A. Calcium accumulation in visual interneurons of the fly: stimulus dependence and relationship to membrane potential. *Journal of neurophysiology* **73**, 2540–2552 (1995). doi: [10.1152/jn.1995.73.6.2540](https://doi.org/10.1152/jn.1995.73.6.2540)
11. Grether, M. E., Abrams, J. M., Agapite, J., White, K. & Steller, H. The head involution defective gene of *Drosophila melanogaster* functions in programmed cell death. *Genes & development* **9**, 1694–1708 (1995). doi: <https://doi.org/10.1101/gad.9.14.1694>
12. Sweeney, S. T., Broadie, K., Keane, J., Niemann, H. & O’Kane, C. J. Targeted expression of tetanus toxin light chain in *Drosophila* specifically eliminates synaptic transmission and causes behavioral defects. *Neuron* **14**, 341–351 (1995). doi: [10.1016/0896-6273\(95\)90290-2](https://doi.org/10.1016/0896-6273(95)90290-2)

13. Chen, P., Nordstrom, W., Gish, B. & Abrams, J. M. grim, a novel cell death gene in Drosophila. *Genes & development* **10**, 1773–1782 (1996). doi: [10.1101/gad.10.14.1773](https://doi.org/10.1101/gad.10.14.1773)
14. Miyawaki, A. *et al.* Fluorescent indicators for Ca<sup>2+</sup> based on green fluorescent proteins and calmodulin. *Nature* **388**, 882–887 (1997). doi: [10.1038/42264](https://doi.org/10.1038/42264)
15. Johns, D. C., Marx, R., Mains, R. E., O'Rourke, B. & Marbán, E. Inducible genetic suppression of neuronal excitability. *Journal of Neuroscience* **19**, 1691–1697 (1999). doi: <https://doi.org/10.1523/JNEUROSCI.19-05-01691.1999>
16. Littleton, J. T. & Ganetzky, B. Ion channels and synaptic organization: analysis of the Drosophila genome. *Neuron* **26**, 35–43 (2000). doi: [10.1016/S0896-6273\(00\)81135-6](https://doi.org/10.1016/S0896-6273(00)81135-6)
17. Kitamoto, T. Conditional modification of behavior in Drosophila by targeted expression of a temperature-sensitive shibire allele in defined neurons. *Journal of neurobiology* **47**, 81–92 (2001). doi: [10.1002/neu.1018](https://doi.org/10.1002/neu.1018)
18. Nagai, T., Sawano, A., Park, E. S. & Miyawaki, A. Circularly permuted green fluorescent proteins engineered to sense Ca<sup>2+</sup>. *Proceedings of the National Academy of Sciences* **98**, 3197–3202 (2001). doi: [10.1073/pnas.051636098](https://doi.org/10.1073/pnas.051636098)
19. Chapman, E. R. Synaptotagmin: a Ca<sup>2+</sup> sensor that triggers exocytosis? *Nature Reviews Molecular Cell Biology* **3**, 498–508 (2002). doi: [10.1038/nrm855](https://doi.org/10.1038/nrm855)
20. Sabatini, B. L., Oertner, T. G. & Svoboda, K. The life cycle of Ca<sup>2+</sup> ions in dendritic spines. *Neuron* **33**, 439–452 (2002). doi: [10.1016/S0896-6273\(02\)00573-1](https://doi.org/10.1016/S0896-6273(02)00573-1)
21. Bennett, M. V. & Zukin, R. S. Electrical coupling and neuronal synchronization in the mammalian brain. *Neuron* **41**, 495–511 (2004). doi: [10.1016/S0896-6273\(04\)00043-1](https://doi.org/10.1016/S0896-6273(04)00043-1)
22. Wilson, R. I., Turner, G. C. & Laurent, G. Transformation of olfactory representations in the Drosophila antennal lobe. *Science* **303**, 366–370 (2004). doi: [10.1126/science.1090782](https://doi.org/10.1126/science.1090782)
23. Gutman, G. A. *et al.* International Union of Pharmacology. LIII. Nomenclature and molecular relationships of voltage-gated potassium channels. *Pharmacological reviews* **57**, 473–508 (2005). doi: [10.1124/pr.57.4.10](https://doi.org/10.1124/pr.57.4.10)
24. Murata, Y., Iwasaki, H., Sasaki, M., Inaba, K. & Okamura, Y. Phosphoinositide phosphatase activity coupled to an intrinsic voltage sensor. *Nature* **435**, 1239–1243 (2005). doi: [10.1038/nature03650](https://doi.org/10.1038/nature03650)
25. King, G. F. Modulation of insect CaV channels by peptidic spider toxins. *Toxicon* **49**, 513–530 (2007). doi: [10.1016/j.toxicon.2006.11.012](https://doi.org/10.1016/j.toxicon.2006.11.012)
26. Di Maio, V. Regulation of information passing by synaptic transmission: a short review. *Brain research* **1225**, 26–38 (2008). doi: [10.1016/j.brainres.2008.06.016](https://doi.org/10.1016/j.brainres.2008.06.016)
27. Joesch, M., Plett, J., Borst, A. & Reiff, D. F. Response properties of motion-sensitive visual interneurons in the lobula plate of Drosophila melanogaster. *Current Biology* **18**, 368–374 (2008). doi: [10.1016/j.cub.2008.02.022](https://doi.org/10.1016/j.cub.2008.02.022)

28. Pfeiffer, B. D. *et al.* Tools for neuroanatomy and neurogenetics in *Drosophila*. *Proceedings of the National Academy of Sciences* **105**, 9715–9720 (2008). doi: [10.1073/pnas.0803697105](https://doi.org/10.1073/pnas.0803697105)
29. Borst, A. *Drosophila's view on insect vision*. *Current biology* **19**, R36–R47 (2009). doi: [10.1016/j.cub.2008.11.001](https://doi.org/10.1016/j.cub.2008.11.001)
30. Gu, H. *et al.* Cav2-type calcium channels encoded by cac regulate AP-independent neurotransmitter release at cholinergic synapses in adult *Drosophila* brain. *Journal of neurophysiology* **101**, 42–53 (2009). doi: [10.1152/jn.91103.2008](https://doi.org/10.1152/jn.91103.2008)
31. Bellen, H. J., Tong, C. & Tsuda, H. 100 years of *Drosophila* research and its impact on vertebrate neuroscience: a history lesson for the future. *Nature Reviews Neuroscience* **11**, 514–522 (2010). doi: [10.1038/nrn2839](https://doi.org/10.1038/nrn2839)
32. Joesch, M., Schnell, B., Raghu, S. V., Reiff, D. F. & Borst, A. ON and OFF pathways in *Drosophila* motion vision. *Nature* **468**, 300–304 (2010). doi: <https://doi.org/10.1038/nature09545>
33. Schnell, B. *et al.* Processing of horizontal optic flow in three visual interneurons of the *Drosophila* brain. *Journal of neurophysiology* **103**, 1646–1657 (2010). doi: [10.1152/jn.00950.2009](https://doi.org/10.1152/jn.00950.2009)
34. Clark, D. A., Bursztyn, L., Horowitz, M. A., Schnitzer, M. J. & Clandinin, T. R. Defining the computational structure of the motion detector in *Drosophila*. *Neuron* **70**, 1165–1177 (2011). doi: [10.1016/j.neuron.2011.05.023](https://doi.org/10.1016/j.neuron.2011.05.023)
35. Eichner, H., Joesch, M., Schnell, B., Reiff, D. F. & Borst, A. Internal structure of the fly elementary motion detector. *Neuron* **70**, 1155–1164 (2011). doi: [10.1016/j.neuron.2011.03.028](https://doi.org/10.1016/j.neuron.2011.03.028)
36. Venken, K. J., Simpson, J. H. & Bellen, H. J. Genetic manipulation of genes and cells in the nervous system of the fruit fly. *Neuron* **72**, 202–230 (2011). doi: [10.1016/j.neuron.2011.09.021](https://doi.org/10.1016/j.neuron.2011.09.021)
37. Jin, L. *et al.* Single action potentials and subthreshold electrical events imaged in neurons with a fluorescent protein voltage probe. *Neuron* **75**, 779–785 (2012). doi: [10.1016/j.neuron.2012.06.040](https://doi.org/10.1016/j.neuron.2012.06.040)
38. Masland, R. H. The neuronal organization of the retina. *Neuron* **76**, 266–280 (2012). doi: [10.1016/j.neuron.2012.10.002](https://doi.org/10.1016/j.neuron.2012.10.002)
39. Schnell, B., Raghu, S. V., Nern, A. & Borst, A. Columnar cells necessary for motion responses of wide-field visual interneurons in *Drosophila*. *Journal of Comparative Physiology A* **198**, 389–395 (2012). doi: [10.1007/s00359-012-0716-3](https://doi.org/10.1007/s00359-012-0716-3)
40. Bahl, A., Ammer, G., Schilling, T. & Borst, A. Object tracking in motion-blind flies. *Nature neuroscience* **16**, 730–738 (2013). doi: [10.1038/nn.3386](https://doi.org/10.1038/nn.3386)
41. Chen, T.-W. *et al.* Ultrasensitive fluorescent proteins for imaging neuronal activity. *Nature* **499**, 295–300 (2013). doi: [10.1038/nature12354](https://doi.org/10.1038/nature12354)
42. Iniguez, J., Schutte, S. S. & O'Dowd, D. K. Cav3-type  $\alpha 1T$  calcium channels mediate transient calcium currents that regulate repetitive firing in *Drosophila* antennal lobe PNs. *Journal of neurophysiology* **110**, 1490–1496 (2013). doi: [10.1152/jn.00368.2013](https://doi.org/10.1152/jn.00368.2013)

43. Joesch, M., Weber, F., Eichner, H. & Borst, A. Functional specialization of parallel motion detection circuits in the fly. *Journal of Neuroscience* **33**, 902–905 (2013). doi: [10.1523/JNEUROSCI.3374-12.2013](https://doi.org/10.1523/JNEUROSCI.3374-12.2013)
44. Lin, J. Y., Knutson, P. M., Muller, A., Kleinfeld, D. & Tsien, R. Y. ReaChR: a red-shifted variant of channelrhodopsin enables deep transcranial optogenetic excitation. *Nature neuroscience* **16**, 1499–1508 (2013). doi: <https://doi.org/10.1038/nn.3502>
45. Maisak, M. S. *et al.* A directional tuning map of Drosophila elementary motion detectors. *Nature* **500**, 212–216 (2013). doi: [10.1038/nature12320](https://doi.org/10.1038/nature12320)
46. Tuthill, J. C., Nern, A., Holtz, S. L., Rubin, G. M. & Reiser, M. B. Contributions of the 12 neuron classes in the fly lamina to motion vision. *Neuron* **79**, 128–140 (2013). doi: [10.1016/j.neuron.2013.05.024](https://doi.org/10.1016/j.neuron.2013.05.024)
47. Behnia, R., Clark, D. A., Carter, A. G., Clandinin, T. R. & Desplan, C. Processing properties of ON and OFF pathways for Drosophila motion detection. *Nature* **512**, 427–430 (2014). doi: [10.1038/nature13427](https://doi.org/10.1038/nature13427)
48. Broussard, G. J., Liang, R. & Tian, L. Monitoring activity in neural circuits with genetically encoded indicators. *Frontiers in molecular neuroscience* **7**, 97 (2014). doi: [10.3389/fnmol.2014.00097](https://doi.org/10.3389/fnmol.2014.00097)
49. Strother, J. A., Nern, A. & Reiser, M. B. Direct observation of ON and OFF pathways in the Drosophila visual system. *Current Biology* **24**, 976–983 (2014). doi: [10.1016/j.cub.2014.03.017](https://doi.org/10.1016/j.cub.2014.03.017)
50. Borst, A. & Helmstaedter, M. Common circuit design in fly and mammalian motion vision. *Nature neuroscience* **18**, 1067–1076 (2015). doi: [10.1038/nn.4050](https://doi.org/10.1038/nn.4050)
51. Govorunova, E. G., Sineshchekov, O. A., Janz, R., Liu, X. & Spudich, J. L. Natural light-gated anion channels: A family of microbial rhodopsins for advanced optogenetics. *Science* **349**, 647–650 (2015). doi: <https://doi.org/10.1126/science.aaa7484>
52. Mauss, A. S., Busch, C. & Borst, A. Optogenetic neuronal silencing in Drosophila during visual processing. *Scientific reports* **7**, 1–12 (2017). doi: <https://doi.org/10.1038/s41598-017-14076-7>
53. Mohammad, F. *et al.* Optogenetic inhibition of behavior with anion channelrhodopsins. *Nature methods* **14**, 271–274 (2017). doi: <https://doi.org/10.1038/nmeth.4148>
54. Busch, C., Borst, A. & Mauss, A. S. Bi-directional control of walking behavior by horizontal optic flow sensors. *Current Biology* **28**, 4037–4045 (2018). doi: <https://doi.org/10.1016/j.cub.2018.11.010>
55. Zheng, Z. *et al.* A complete electron microscopy volume of the brain of adult Drosophila melanogaster. *Cell* **174**, 730–743 (2018). doi: [10.1016/j.cell.2018.06.019](https://doi.org/10.1016/j.cell.2018.06.019)
56. Piggott, B. J. *et al.* Paralytic, the Drosophila voltage-gated sodium channel, regulates proliferation of neural progenitors. *Genes & development* **33**, 1739–1750 (2019). doi: [10.1101/gad.330597.119](https://doi.org/10.1101/gad.330597.119)
57. Luo, L. *Principles of Neurobiology* (Garland Science, 2020). doi: [10.1201/9781003053972](https://doi.org/10.1201/9781003053972)
58. Ammer, G., Vieira, R. M., Fendl, S. & Borst, A. Anatomical distribution and functional roles of electrical synapses in Drosophila. *Current Biology* **32** (2022). doi: [10.1016/j.cub.2022.03.040](https://doi.org/10.1016/j.cub.2022.03.040)